AD-A085 344 PURDUE UNIV LAFAYETTE IND SCHOOL OF MECHANICAL ENGI--ETC F/G 20/4
LASER VELOCIMETER MEASUREMENTS IN TURBULENT AND MIXING FLOWS. P--ETC(U)
MAR 80 W H STEVENSON, H D THOMPSON, R BREMMER F33615-77-C-2010
UNCLASSIFIED AFAPL-TR-79-2009-PT-2 NL

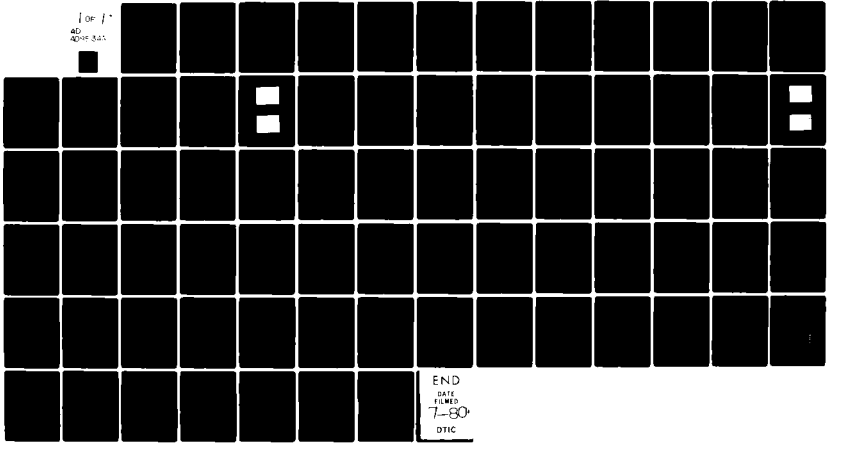

AFAPL-TR-79-2009

Part II

LASER VELOCIMETER MEASUREMENTS IN TURBULENT AND MIXING FLOWS - PART II

W. H. STEVENSON
H. DOYLE THOMPSON
ROBIN BREMMER
TIMOTHY ROESLER

SCHOOL OF MECHANICAL ENGINEERING
PURDUE UNIVERSITY
WEST LAFAYETTE, INDIANA 47907

MARCH 1980

TECHNICAL REPORT AFAPL-TR-79-2009, Part II
Interim Technical Report for Period October 1978 - December 1979

Approved for public release; distribution unlimited.

AERO PROPULSION LABORATORY
AIR FORCE WRIGHT AERONAUTICAL LABORATORIES
AIR FORCE SYSTEMS COMMAND
WRIGHT-PATTERSON AIR FORCE BASE, OHIO 45433

NOTICE

When Government drawings, specifications, or other data are used for any purpose other than in connection with a definitely related Government procurement operation, the United States Government thereby incurs no responsibility nor any obligation whatsoever; and the fact that the government may have formulated, furnished, or in any way supplied the said drawings, specifications, or licensing the holder or any other person or corporation, or conveying any rights or permission to manufacture, use, or sell any patented invention that may in any way be related thereto.

This report has been reviewed by the Information Office (ASD/OIP) and is releasable to the National Technical Information Services (NTIS). At NTIS, it will be available to the general public, including foreign nations.

This technical report has been reviewed and is approved for publication.

Roger R. Craig
Project Engineer

Frank D. Stull, Chief
Ramjet Technology Branch
Ramjet Engine Division

FOR THE COMMANDER

Edward T. Curran

E.T. Curran, Deputy Director
Ramjet Engine Division

Copies of this report should not be returned unless return is required by security considerations, contractual obligations, or notice on a specific document.

AIR FORCE/56780/27 May 1980 — 100

(17) TR-79-2009-PT-2

SECURITY CLASSIFICATION OF THIS PAGE (When Data Entered)

REPORT DOCUMENTATION PAGE

READ INSTRUCTIONS BEFORE COMPLETING FORM

1. REPORT NUMBER (18) AFAPL-TR-79-2009 Part II	2. GOVT ACCESSION NO. AD-A085344
3. RECIPIENT'S CATALOG NUMBER	
4. TITLE (and Subtitle) (6) LASER VELOCIMETER MEASUREMENTS IN TURBULENT AND MIXING FLOWS, PART II.	5. TYPE OF REPORT & PERIOD COVERED Interim: 1 Oct. 1978 - 15 Dec. 1979
	6. PERFORMING ORG. REPORT NUMBER
7. AUTHOR(s) W.H. Stevenson, H. Doyle Thompson, Robin Bremmer, and Timothy Roesler	8. CONTRACT OR GRANT NUMBER(s) (15) F33615-77-C-2010
9. PERFORMING ORGANIZATION NAME AND ADDRESS School of Mechanical Engineering, Purdue University, West Lafayette, Indiana	10. PROGRAM ELEMENT, PROJECT, TASK AREA & WORK UNIT NUMBERS (16) 2308/S1-02 (17) S1L
11. CONTROLLING OFFICE NAME AND ADDRESS (11) Aero Propulsion Laboratory (PORT), Air Force Wright Aeronautical Laboratories (AFSC), Wright-Patterson Air Force Base, Ohio 45433	12. REPORT DATE Mar 80
	13. NUMBER OF PAGES 64
14. MONITORING AGENCY NAME & ADDRESS (if different from Controlling Office) (9) Interim rept. 1 Oct 78 - 15 Dec 79,	15. SECURITY CLASS. (of this report) UNCLASSIFIED
	15a. DECLASSIFICATION/DOWNGRADING SCHEDULE

16. DISTRIBUTION STATEMENT (of this Report)

Approved for public release; distribution unlimited. (12) 75

17. DISTRIBUTION STATEMENT (of the abstract entered in Block 20, if different from Report)

(10) Warren H. / Stevenson H. Doyle / Thompson Robin / Bremmer Timothy / Roesler

18. SUPPLEMENTARY NOTES

19. KEY WORDS (Continue on reverse side if necessary and identify by block number)

Turbulence measurements
Laser velocimeter
Bias errors (in laser velocimetry)

20. ABSTRACT (Continue on reverse side if necessary and identify by block number)

An experimental and analytical study of subsonic flow over a rearward facing step is reported. A major emphasis of the work is the investigation of bias errors in mean velocities obtained from laser doppler velocimeter (LDV) measurements in such highly turbulent flows. Optical alignment of the specially designed LDV used in the study is described in detail. An analysis of the biasing problem is presented and preliminary measurements

Page 1

DD FORM 1 JAN 73 1473 EDITION OF 1 NOV 65 IS OBSOLETE
S/N 0102-014-6601 |

SECURITY CLASSIFICATION OF THIS PAGE (When Data Entered)

which appear to confirm previously predicted velocity bias errors are reported. Results of a computer model developed to describe the flow are presented together with preliminary static pressure measurements made in the flow facility.

PREFACE

This interim report was submitted by the School of Mechanical Engineering of Purdue University, under Contract No. F33615-77-C-2010 and covers the period 1 October 1978-15 December 1979. The effort was sponsored by the Aero Propulsion Laboratory, Air Force Wright Aeronautical Laboratories, Wright-Patterson AFB, Ohio under Project No. 2308 with Roger R. Craig/AFWAL/PORT as Project Engineer. Warren H. Stevenson and H. Doyle Thompson of Purdue University were technically responsible for the work.

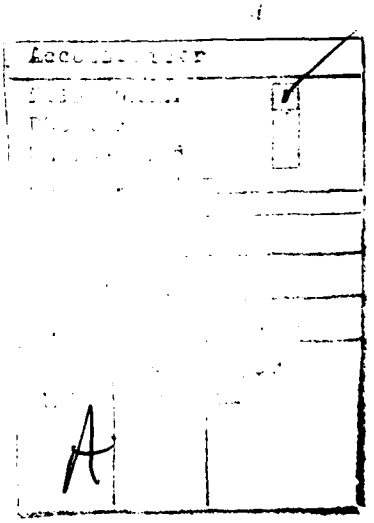

TABLE OF CONTENTS

TABLE OF CONTENTS

(continued)

LIST OF ILLUSTRATIONS

LIST OF ILLUSTRATIONS
(Continued)

NOMENCLATURE

C_1, C_2, C_D	turbulence constants
$\hat{e}_x, \hat{e}_y, \hat{e}_z$	unit vectors in the x, y, and z directions
$\hat{e}_1, \hat{e}_2$	unit vectors along incident intersecting beams
$\hat{e}_n$	unit vector normal to bisector and in the plane of incident intersecting beams
$\hat{e}_t$	unit vector tangent to bisector and in the plane of incident intersecting beams
G_k	see equation 57
h	step height
k	kinetic energy of turbulence
n	refractive index of medium
P	static pressure
P_o	upstream (reference) static pressure
U_o	upstream (reference) velocity in x-direction
u	$\overline{u} + u' = \langle u \rangle + u^*$, velocity in x-direction
v	$\overline{v} + v' = \langle v \rangle + v^*$, velocity in y-direction
w	$\overline{w} + w' = \langle w \rangle + w^*$, velocity in z-direction
$\overline{u'v'}$	Reynolds stress
$\vec{V}$	$u\hat{e}_x + v\hat{e}_y + w\hat{e}_z$, total velocity vector
ε	rate of dissipation of turbulence kinetic energy (k)
ε_T	total laser Doppler system bias
ε^*	velocity bias
ε^{**}	incomplete signal bias
λ_o	wavelength of laser light
μ	fluid viscosity

μ_t	turbulent viscosity
ν	$\overline{\nu} + \nu' = \langle\nu\rangle + \nu^*$, measured Doppler frequency
ν_s	frequency shift introduced into one of incident intersecting beams
ρ	fluid density
σ_k	turbulent Prandtl number for k
σ_ε	turbulent Prandtl number for ε
θ	angle between incident intersecting beams
ϕ	angle between $\hat{e}_n$ and $\hat{e}_x$ (see Figure 15). ϕ is the angle of rotation of the optical system about its axis, the $\hat{e}_y$ direction
ψ^*	non-dimensionalized stream function
$[\ ]_\phi$	quantity evaluated at ϕ
$\overline{\ }$,'	time average and its fluctuation quantity
$\langle\ \rangle$,*	ensemble average and its fluctuation quantity

SECTION I

INTRODUCTION

The primary objective of this research program is to investigate the application of laser Doppler velocimetry to turbulent and mixing flows. Of particular interest are the bias errors which have been predicted for such flows. The experimental verification of such errors has proven to be difficult and a number of studies have produced conflicting results. Therefore a variable probe volume laser velocimeter has been designed to permit a careful study of the biasing problem. The design of this LDV system and the two-dimensional flow facility fabricated for the experiments were described in the previous annual report [1].

A secondary objective of the research is to investigate the feasibility of using fluorescent particles in studies of turbulent mixing. In addition the program has been extended to include mapping of the flow field in a cold flow model of a dump combustor. The mixing studies will be conducted during the next phase of the work and are not reported here.

Section II of the present report outlines the rather extensive procedures used to optimize the optical alignment of the LDV and accurately determine probe volume characteristics. Section III presents a new analysis of the biasing problem which offers a theoretical basis for determining bias errors from discrete velocity measurements. Preliminary data on velocity bias in a turbulent flow are presented in Section IV. These data indicate a bias which agrees well with previous theoretical predictions. The results of a detailed computer prediction for flow over a step which models our flow facility are presented in Section V, together with some preliminary experimental data on static wall pressures. This computer program can readily be extended to the axisymmetric dump combustor model which will be studied during the next phase of the work.

---

[1] Stevenson, W.H. and Thompson, H.D., "Laser Velocimeter Measurements in Turbulent and Mixing Flows," AFAPL-TR-79-2009, March 1979.

SECTION II

LDV ALIGNMENT AND ADJUSTMENTS

1. System Design

The LDV system was designed specifically for studying various bias errors. It has provisions for changing the probe volume size, the fringe spacing, and the angular orientation of the probe volume. It is also possible to frequency shift the beams with a dual Bragg cell system. The general layout of the device is shown in Figure 1. The flexibility of this system allows the probe volume characteristics to be varied over a wide range. However, it also requires a rather careful alignment to insure that the desired conditions are obtained.

Laser light for the system is supplied by a 5 watt Argon laser. The beam exits the laser and enters a polarization rotator. The polarization rotator insures maximum fringe contrast in the probe volume. Following the polarization rotator is the beam expander telescope. The telescope is composed of a 44 mm lens (f_1) followed by a 68 mm lens (f_2). The f_1 lens images the beam waist from inside the laser cavity to a point between the two telescope lenses. Then lens f_2 and the transmitting lens image this waist to a location within the test region. Waist diameters of 60 to 500 μm can be obtained within the test region by moving f_2 over a 7.5 mm traverse.

From the telescope, the beam is reflected to the upper portion of the transmitting optics package where it enters the beam splitter. The beam splitter is a commercial TSI model #916-1 which splits the entering beam into two parallel equal intensity beams separated by 50 mm.

Following the beam splitter are the two acousto-optic modulators. The modulators shift the frequency of the incoming beam either up or down by an amount equal to the frequency of the driver. Drivers of 30 and either 35 or 40 MHz are used. (Selection of a 35 or 40 MHz shift involves changing the crystal oscillator in the driver.) By using various combinations to shift one or both beams, net frequency upshifts or downshifts of 0, 5, 10, 30, 35, 40, 70, or 75 MHz are available.

Next the beams are reflected by the adjustable mirrors to the sliding prism. The prism directs the beams to the transmitting lens. Various beam separations can be obtained by translating the prism. The adjustable mirrors are used to position the beams so that they cross on the optical axis and at the beam waist. Thus fringe spacing may be changed through proper adjustment of the sliding prism and adjustable mirrors. The transmitting lens has a focal length of 250 mm.

The receiving lenses are a 250 mm lens, similar to the transmitting lens, and a 120 mm lens mounted several centimeters apart. The receiving lenses and the entire receiving optics package may be moved along the axis of the optical system to allow proper focusing.

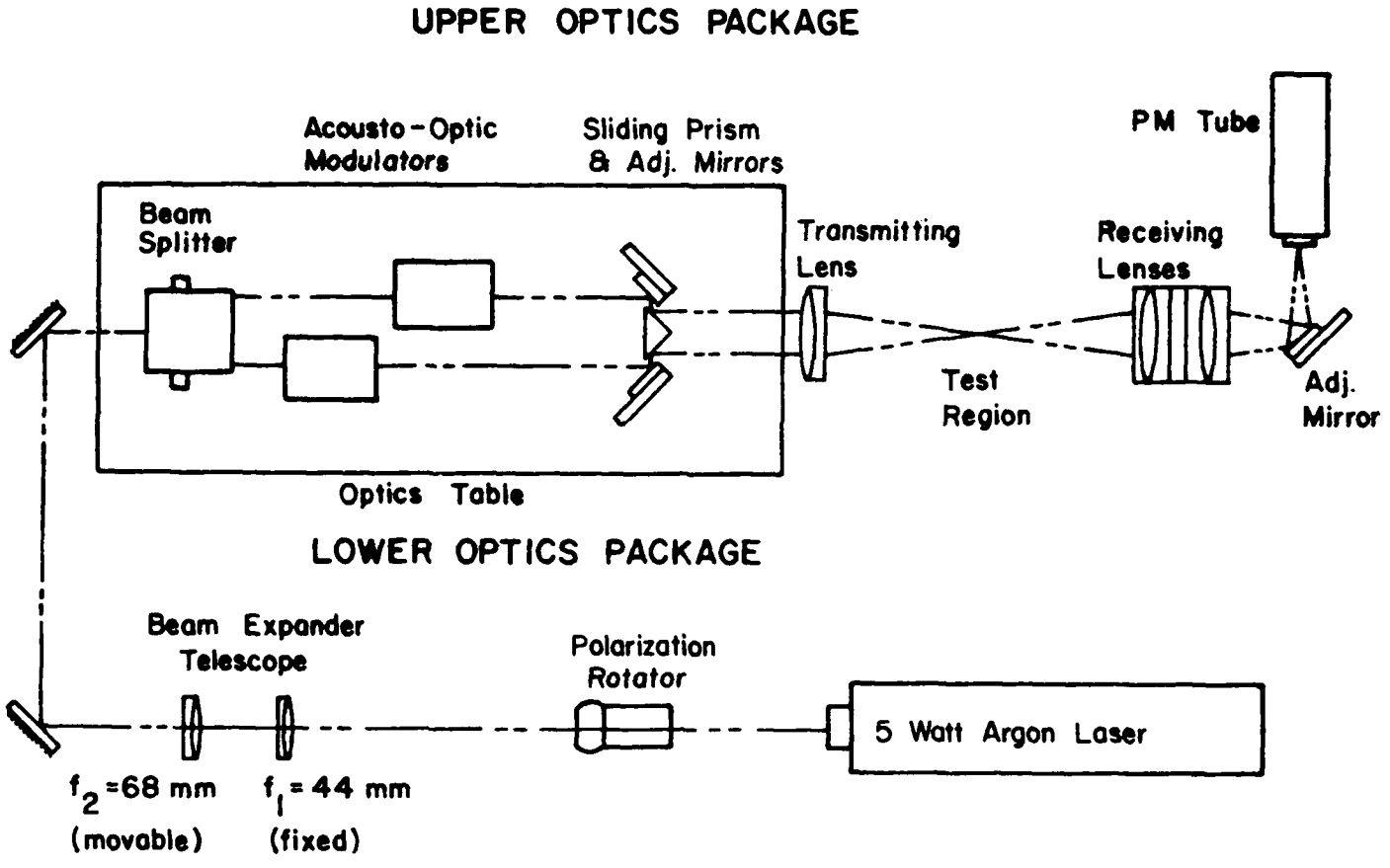

Figure 1. LDV System Diagram

The optics table is mounted in bearings which rotate on the optical axis. Rotation of the optics table rotates the probe volume so that velocity components at various angles to the horizontal can be measured.

2. Experimental Measurement of Beam Waist Diameter and Position

When studying biasing errors, it is essential that the optics by properly aligned and adjusted and that the parameters of the system be accurately known. The beams must be aligned such that they cross on the optical axis and at the waist. These adjustments insure that the fringes within the probe volume are both parallel and of constant width, and that the position of the probe volume does not change as the optics are rotated. To accomplish this, the position of the beam waist must be located and its size determined.

The beam waist position and size for each beam were determined experimentally by the rotating disk method described by Suzaki and Tachibana [2]. The technique involves using a photodiode to measure the change in intensity of the laser beam as it is chopped by a razor blade attached to a rotating disk as illustrated in Figure 2. If the radius of the disk is large compared to the beam diameter, then the $1/e^2$ radius of the beam, w_o, is

$$w_o = 0.7803\,\omega\, r\, \Delta t_{10\text{-}90} \qquad (1)$$

where ω is the angular velocity of the disk in radians per second, r is the distance from the center of rotation of the disk to the laser beam and $\Delta t_{10\text{-}90}$ is the time for the intensity of the beam to drop from 90% to 10% of the maximum. A disk speed of 6.41 radians per second and a radius of 76.0 mm were used.

The position of the beam waist was found by slowly scanning the rotating razor blade along the beam until $\Delta t_{10\text{-}90}$ was a minimum. This is most easily accomplished by viewing the output of the photodiode on a storage oscilloscope set to store multiple traces. A typical group of multiple traces made during a scan is shown in Figure 3. The diameter of the beam at that point is determined from Eq. (1) using the $\Delta t_{10\text{-}90}$ time measured from an expanded single trace similar to Figure 4. This process was repeated three times for each setting of the telescope, and the resulting diameters and waist positions averaged. The diameter measurements for a given telescope setting varied no more than 5.2% with an average variation of about 2.5%. The three waist position measurements at a given setting were typically within a few millimeters of one another.

---

[2] Suzaki, Yasuzi and Tachibana, Atsushi, "Measurements of μm Sized Radius of Gaussian Laser Beam using the Scanning Knife-Edge," Applied Optics, Vol. 14, No. 12, December 1975.

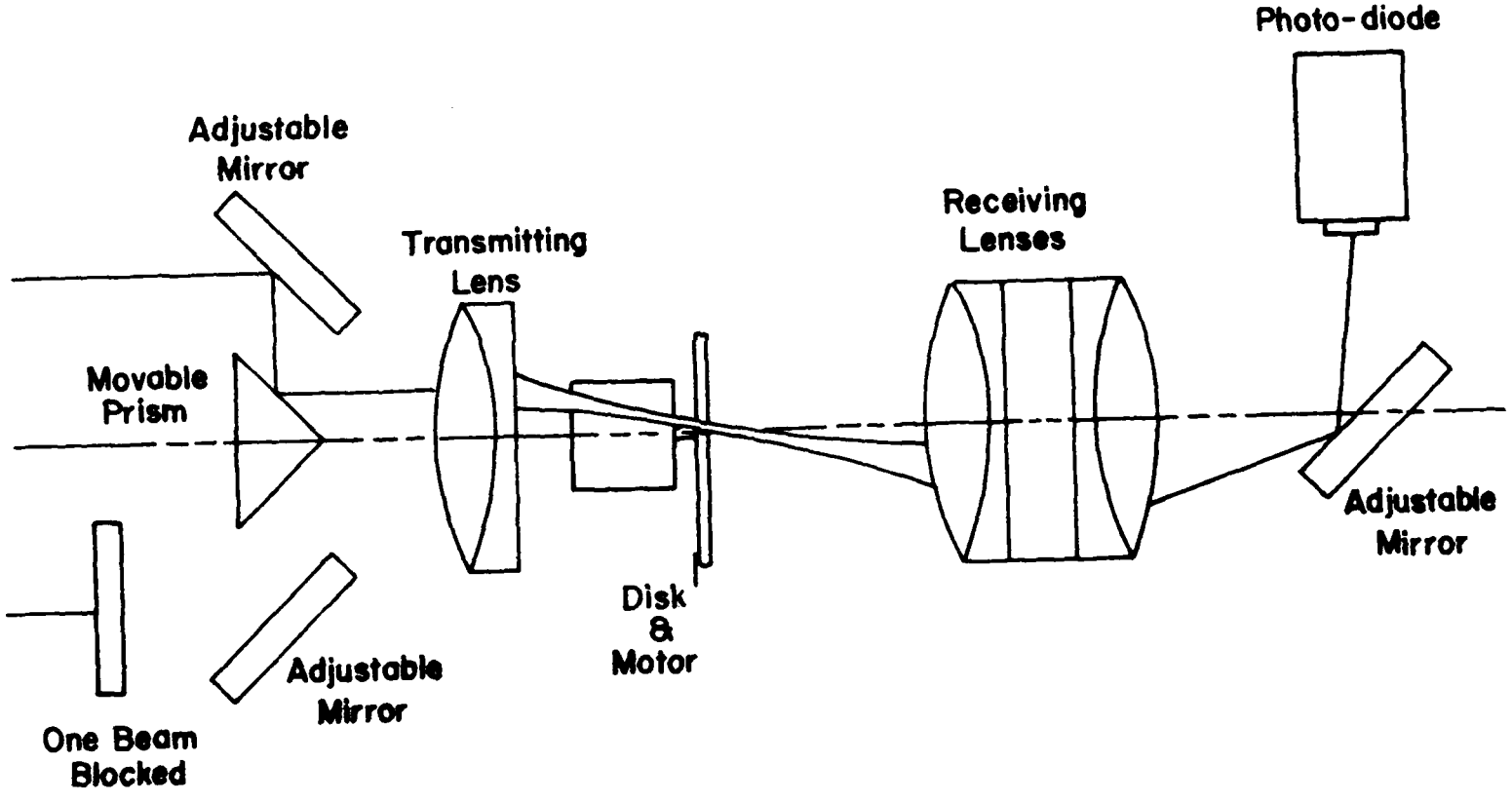

Figure 2. Setup for Measuring Beam Waist and Position

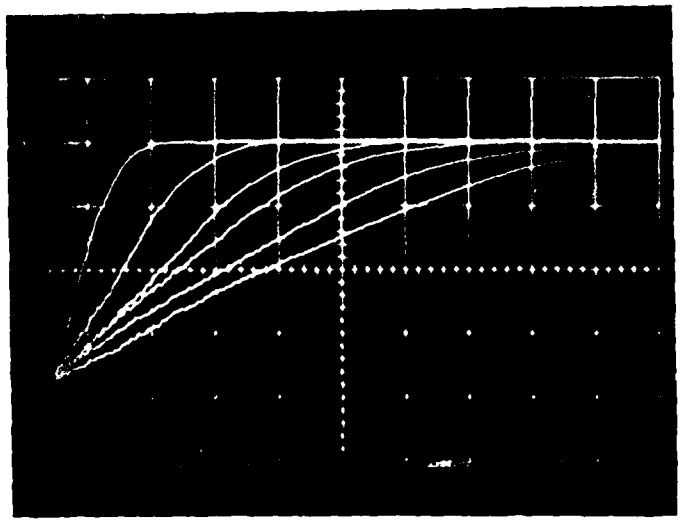

Figure 3. Photodiode Signal from Multiple Knife-Edge Scans

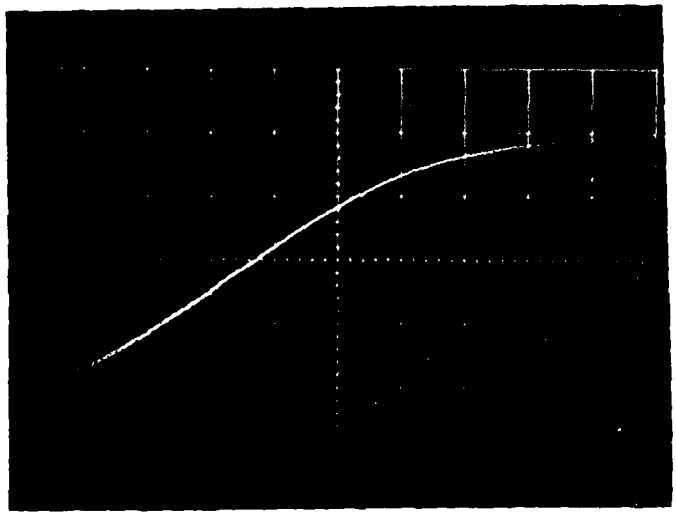

Figure 4. Photodiode Signal from Single Knife-Edge Scan

This scanning technique was found to be quite accurate for beams with waist diameters less than about 250 μm. Above 250 μm, the divergence of the beam becomes very small, and it becomes difficult to measure the waist location by observing the change in the oscilloscope trace during the scan. Therefore, a slightly different technique was used to find the waist size and location in the larger beams.

The portion of the beam where the waist occurs, a span of about 300 mm, was divided into 50 mm increments. The beam was measured several times at each increment and the results averaged. Examination of the data revealed a slight decrease and then increase in beam diameter as one moves down the beam. The region where the beam appeared the smallest was further subdivided and more measurements made. Using this technique, the waist location was determined to within a few millimeters and its diameter found to within several percent. Fortunately, extremely accurate knowledge of waist location is not as necessary for larger beams as it is for the smaller, highly divergent beams.

The results of the beam sizing are shown in Figures 5 and 6. The system can be adjusted to produce probe volumes with diameters of 57 to 490 μm in unfrequency shifted beams. Due to the limited size of the acoustical-optical field height in the acousto-optical modulators, the minimum diameter of the frequency shifted beams is 97 μm due to diffraction effects. The position of the waist ranged from 159 to 275 mm from the face of the transmitting optics lens. Also, it was found that the position of the waist moves steadily towards the transmitting lens for waist sizes up to about 160 μm (telescope setting of 0.250). At some diameter beyond 160 μm a jump occurs causing the waist position to move out several hundred millimeters from the transmitting lens. After the jump the waist position moves steadily towards the transmitting lens as before, but with decreasing waist size. The phenomenon was both observed during testing and predicted by a computer program. Once the position of the beam waist diameter had been determined for various telescope settings, the final alignment could be made.

3. Theoretical Calculation of Beam Waist Diameter and Position

A computer program was developed to verify the waist size and position measurements. The program was designed to image a waist of known size and position thru all lenses to a new waist in the test region. The equations used in the program were given in [3].

$$z_2 = f + \frac{(z_1 - f)f^2}{(z_1 - f)^2 + \left(\frac{\pi w_{o_1}^2}{\lambda}\right)^2} \qquad (2)$$

[3] Weicher, H. and Pedrotti, L.S., "A Summary of Useful Laser Equations an LIA Report," Air Force Institute of Technology, Wright Patterson AFB.

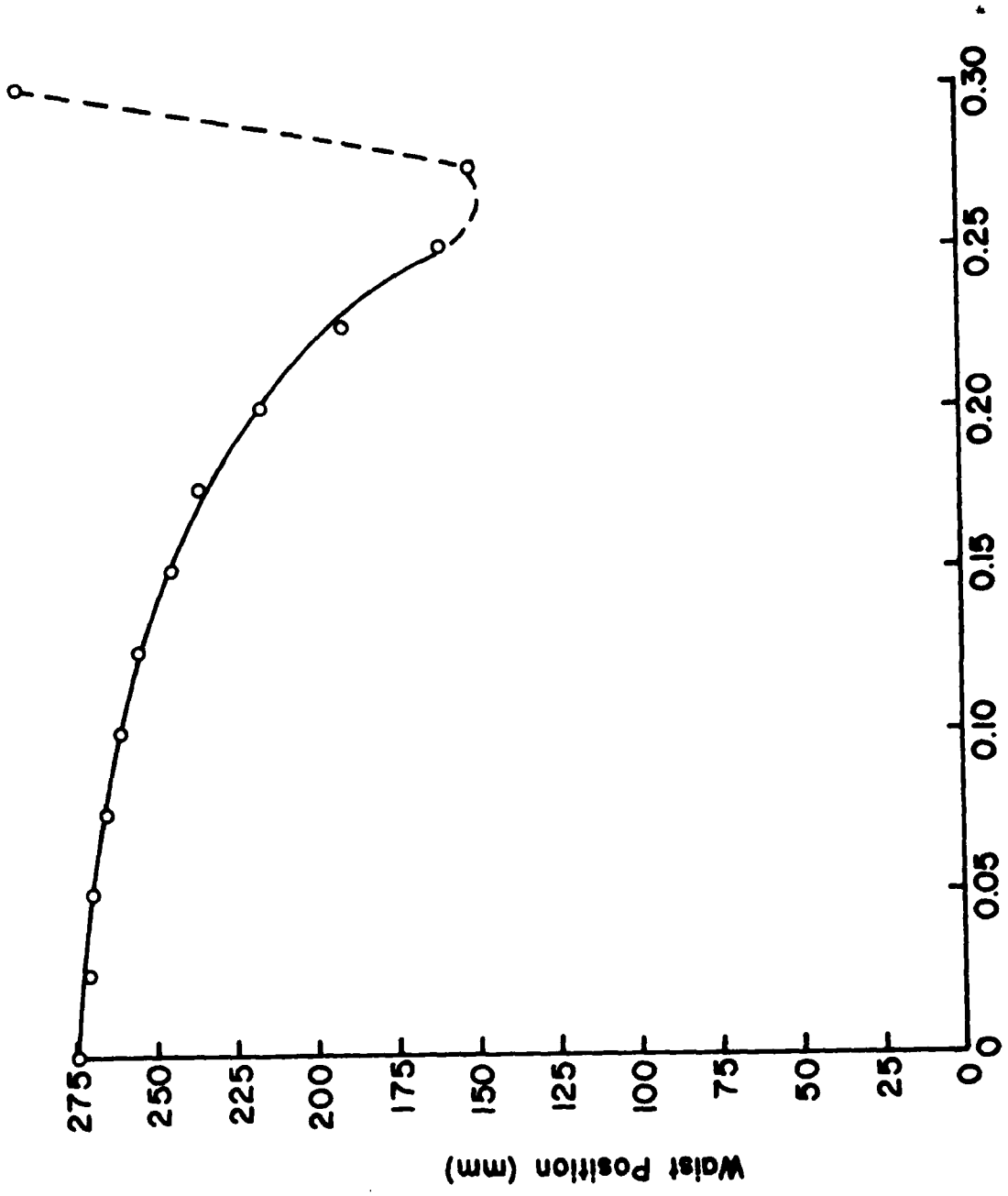

Figure 5. Waist Position vs Telescope Setting

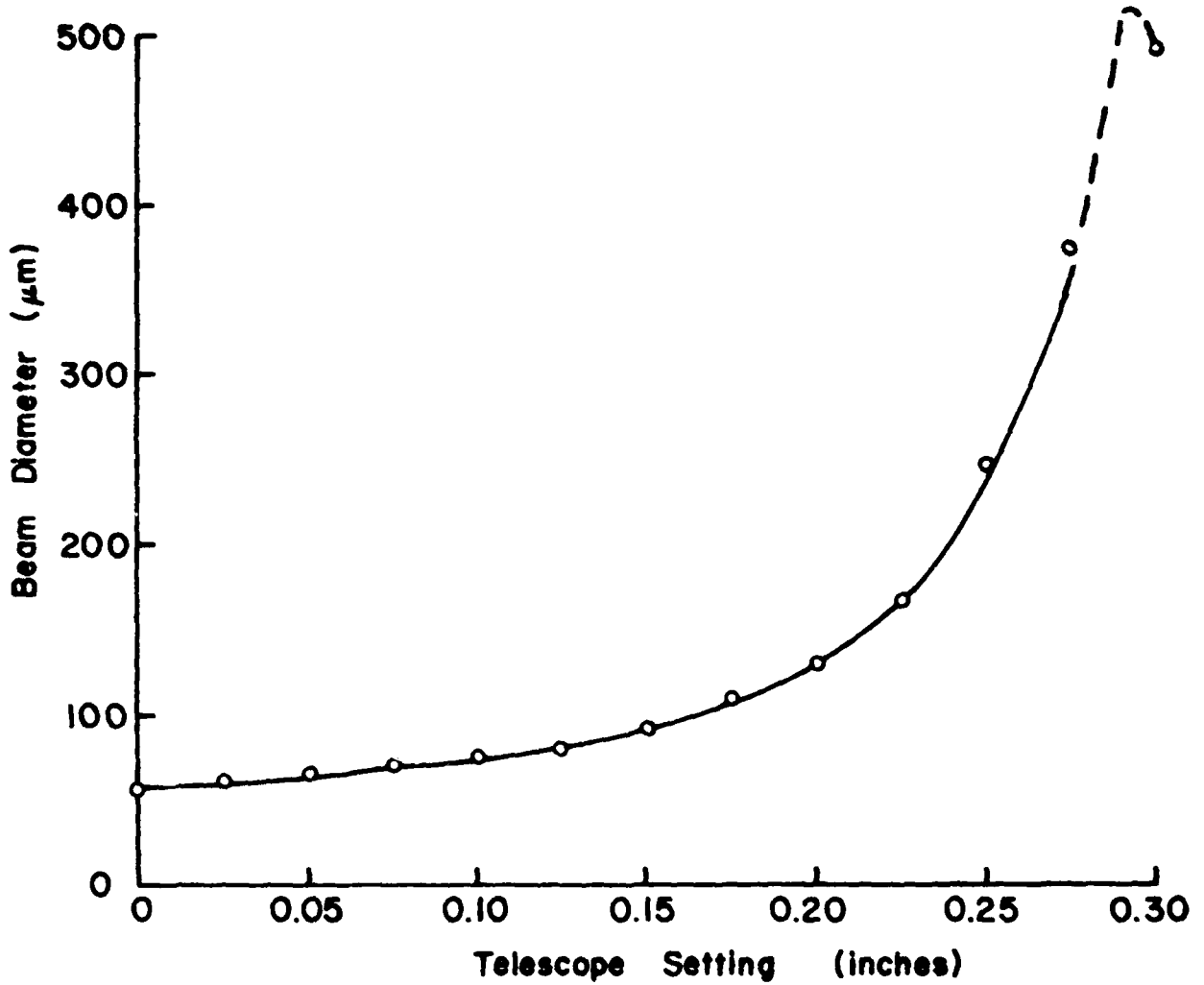

Figure 6. Beam Diameter vs Telescope Setting

$$\frac{1}{w_{o_2}^2} = \frac{1}{w_{o_1}^2}\left(1 - \frac{z_1}{f}\right)^2 + \frac{1}{f^2}\left(\frac{\pi w_{o_1}}{\lambda}\right)^2 \qquad (3)$$

where f is the focal length of the lens, z_1 and w_{o1} are the position and radius of the waist being imaged, z_2 and w_{o2} are the position and radius of the new waist, and λ is the wave length of the laser light.

The diameter and position of the waist occurring between the two lenses of the telescope is highly divergent and easy to measure accurately. Also, it does not change size or position with changes in the optical adjustments. Therefore, this waist was measured by the knife edge scan method described earlier, and this information was used for initial data in the computer program.

The input waist is imaged through lens f_2 of the telescope (see Figure 1) by the above equations to a new waist. This waist is imaged by the transmitting lens to a waist in the test region. The program calculated waist sizes and positions for 0.25 inch increments of telescope lens separation, starting with an initial separation of approximately 211 mm. The optical path length from f_2 to the transmitting lens was measured to be approximately 1550 mm. The program was run using an optical path length of 1550 mm and the initial lens separation was varied until the programs waist diameter at a telescope setting of zero matched the experimentally determined diameter at zero.

The results of the program are shown in Figures 7 and 8. The program predicted that the waist size increases and waist position moves towards the transmitting lens with increasing telescope settings. However, at a telescope setting of approximately 0.225 from the initial setting, the waist moves quickly away from the lens. Increased telescope settings beyond this point result in smaller beam diameters with the waist moving towards the transmitting lens as before. A comparison of the experimental and calculated data shows that both have the same trends, even though the numerical values are not the same. The reason for this discrepancy is probably a result of aberrations which make such a simple analysis inaccurate. The experimental curves are assumed to define actual system behavior.

4. Beam Intersection Alignment

Proper beam intersection is obtained by setting the two adjustable mirrors on either side of the sliding prism such that the beams cross on the optical axis and at the beam waists. Generally, these settings vary depending on both the telescope setting and the prism setting. The angle between the beams must also be measured at this time so that fringe spacing can be calculated.

The alignment technique uses the system shown in Figure 9 and is similar to the one used in measuring the beam diameter and waist position. Alignment is started by placing the rotating disk perpendicular to the beams at the beam

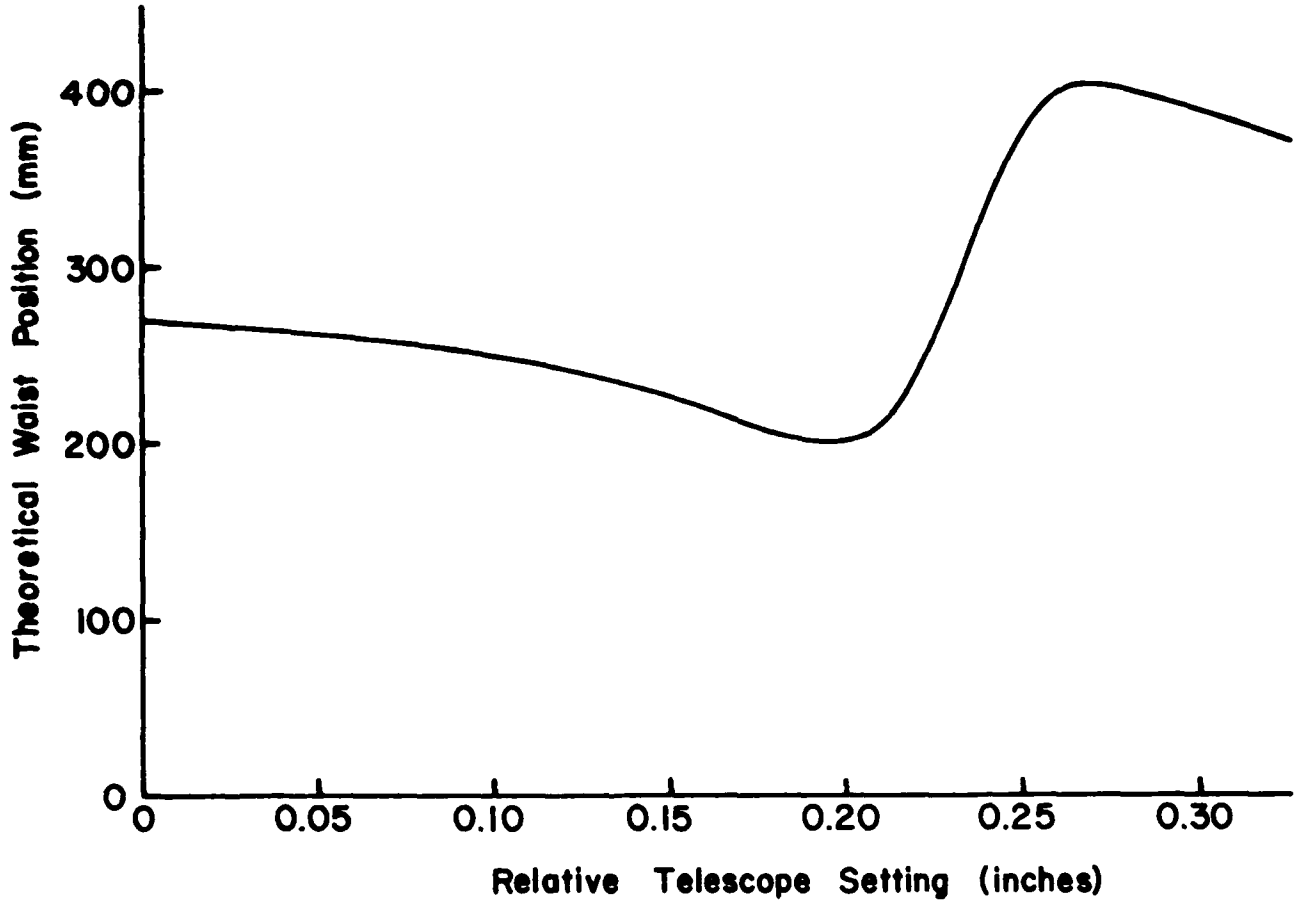

Figure 7. Theoretical Waist Position vs Telescope Setting

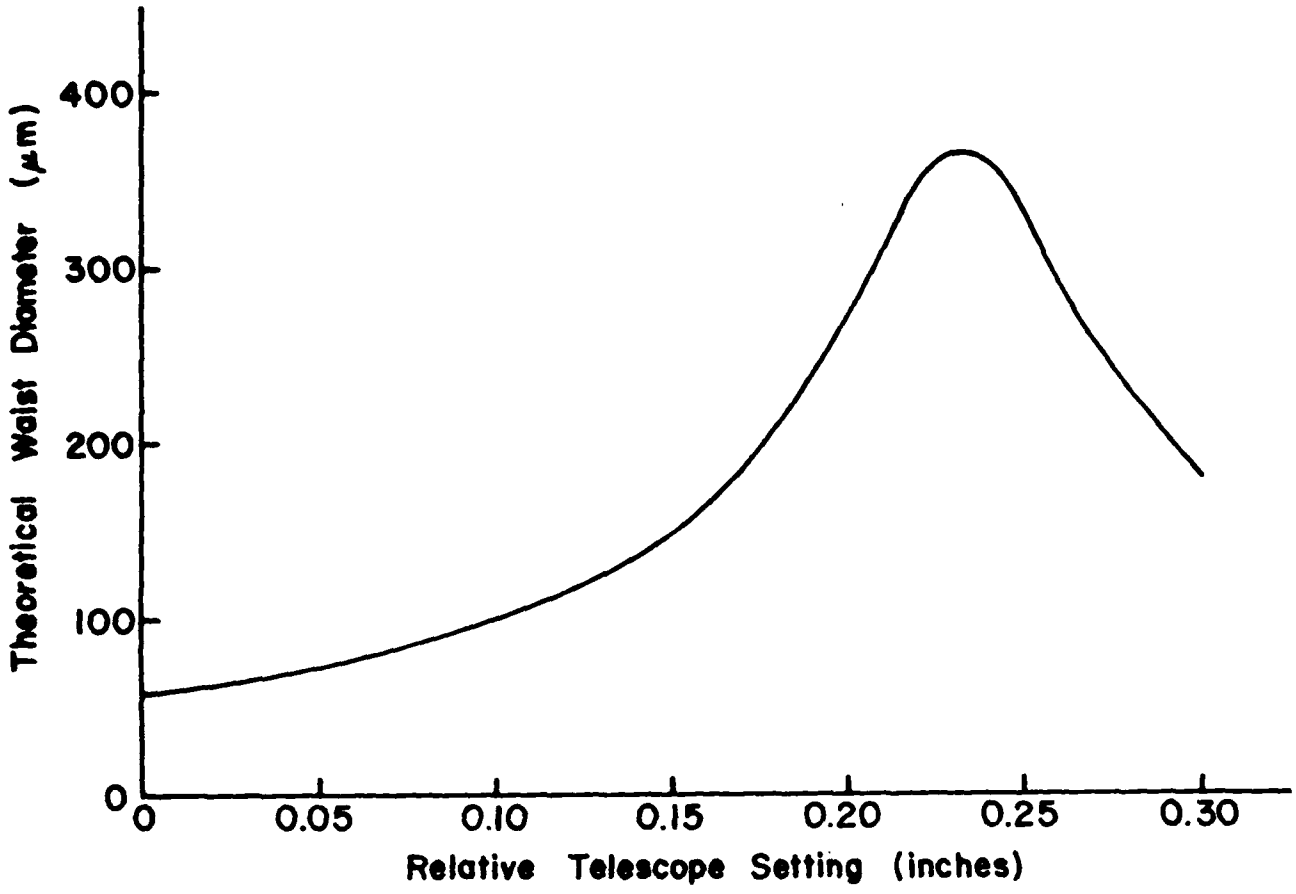

Figure 8. Theoretical Waist Diameter vs Telescope Setting

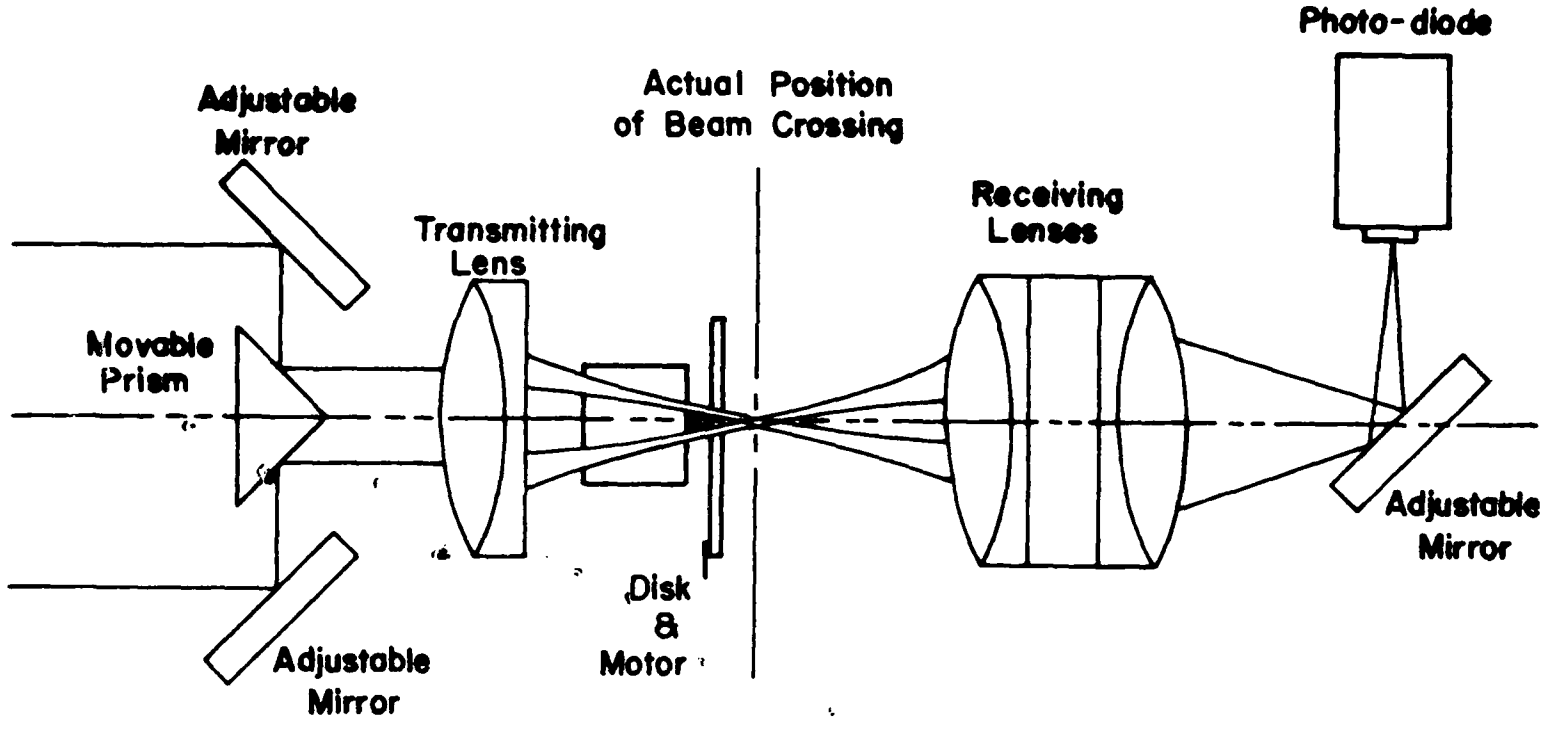

Figure 9. Setup for Alignment of Optics

waist. With the chopper turned off and the razor blade positioned in the beams, the mirrors were adjusted until the beams met in a single point on the blade and until the point remained visibly stationary as the optics were rotated. Next, a photodiode was positioned behind the receiving optics, such that both beams fell on it and the chopper was turned on. If the beams are chopped at the crossing point, the resulting oscilloscope trace will look similar to those produced when sizing single beams. If the blade chops the beams at some point other than the crossing, the trace will be similar to that of a chopped single beam except that it has a small, flat plateau at its center as shown in Figure 10. The beams may be made to cross at the blade by carefully adjusting the two lower micrometer heads on the adjustable mirrors equal amounts but in opposite directions until the plateau is eliminated, as shown in Figure 11. The two mirrors are adjusted by equal amounts to maintain the beam crossing point on the optical axis.

With the mirrors properly adjusted, the settings on the adjustable mirrors are recorded. The chopper is removed from the beams, and a mirror is placed at the crossing point to reflect the beams to a screen. The separation between the beams at the screen and the distance from the screen to the crossing are measured. The half angle and fringe spacing are calculated from this information by

$$\frac{\theta}{2} = \tan^{-1}\left(\frac{x/2}{y}\right) \tag{4}$$

$$\Delta x = \frac{\lambda}{2 \sin \theta/2} \tag{5}$$

Where $\theta/2$ is the half angle between the beams, x and y are the distances shown in Figure 12, Δx is the fringe spacing, and λ is the wavelength of the laser light.

The adjustments described above are most easily made by setting the telescope and then finding the proper mirror adjustments for various prism settings, since the adjustable mirror settings vary linearly with the prism setting. Thus, once the first two sets of adjustments are determined, a pattern is established for approximating the remaining prism settings. As shown in Figure 13, the system can produce fringe spacings ranging from 5 to 15 μm.

Upon completion of the calibrations, plots were drawn such that the proper settings for various combinations of probe volume size, fringe spacing, and frequency shift can be easily determined. (Frequency shifting affects the results slightly due to the small angular shift introduced by the Bragg cell.)

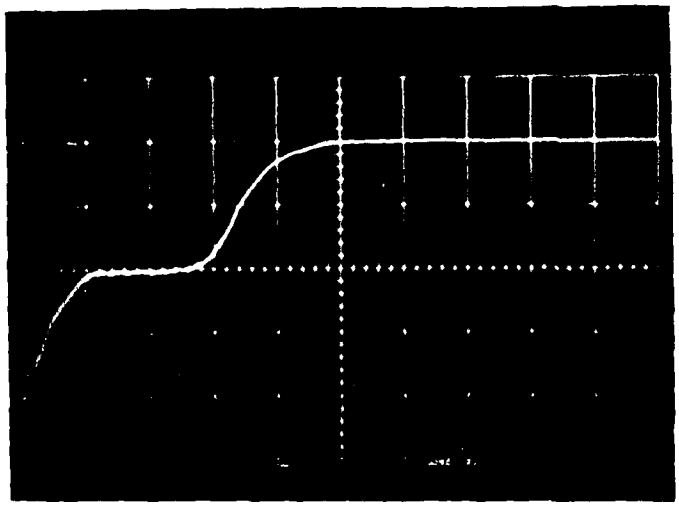

Figure 10. Photodiode Signal from Two Improperly Adjusted Beams

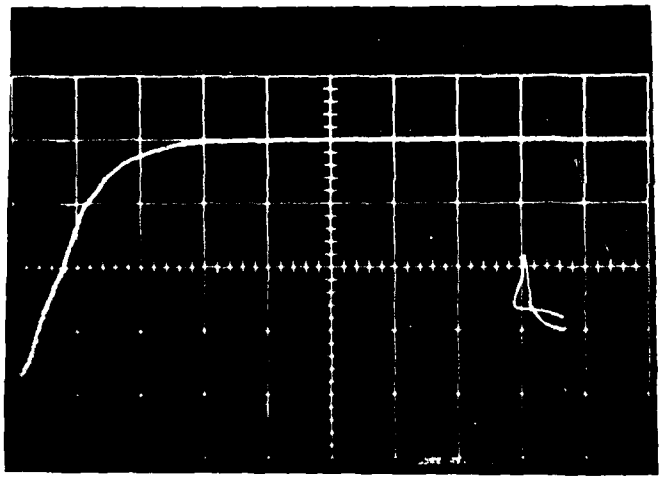

Figure 11. Photodiode Signal for Two Properly Adjusted Beams

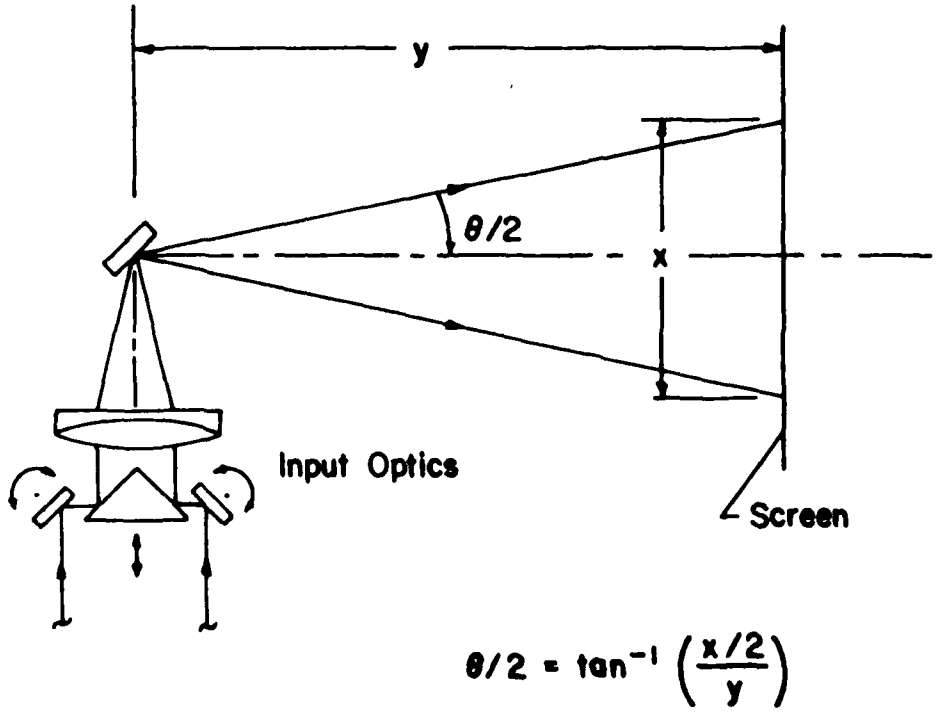

Figure 12. Setup for Measuring Beam Angles

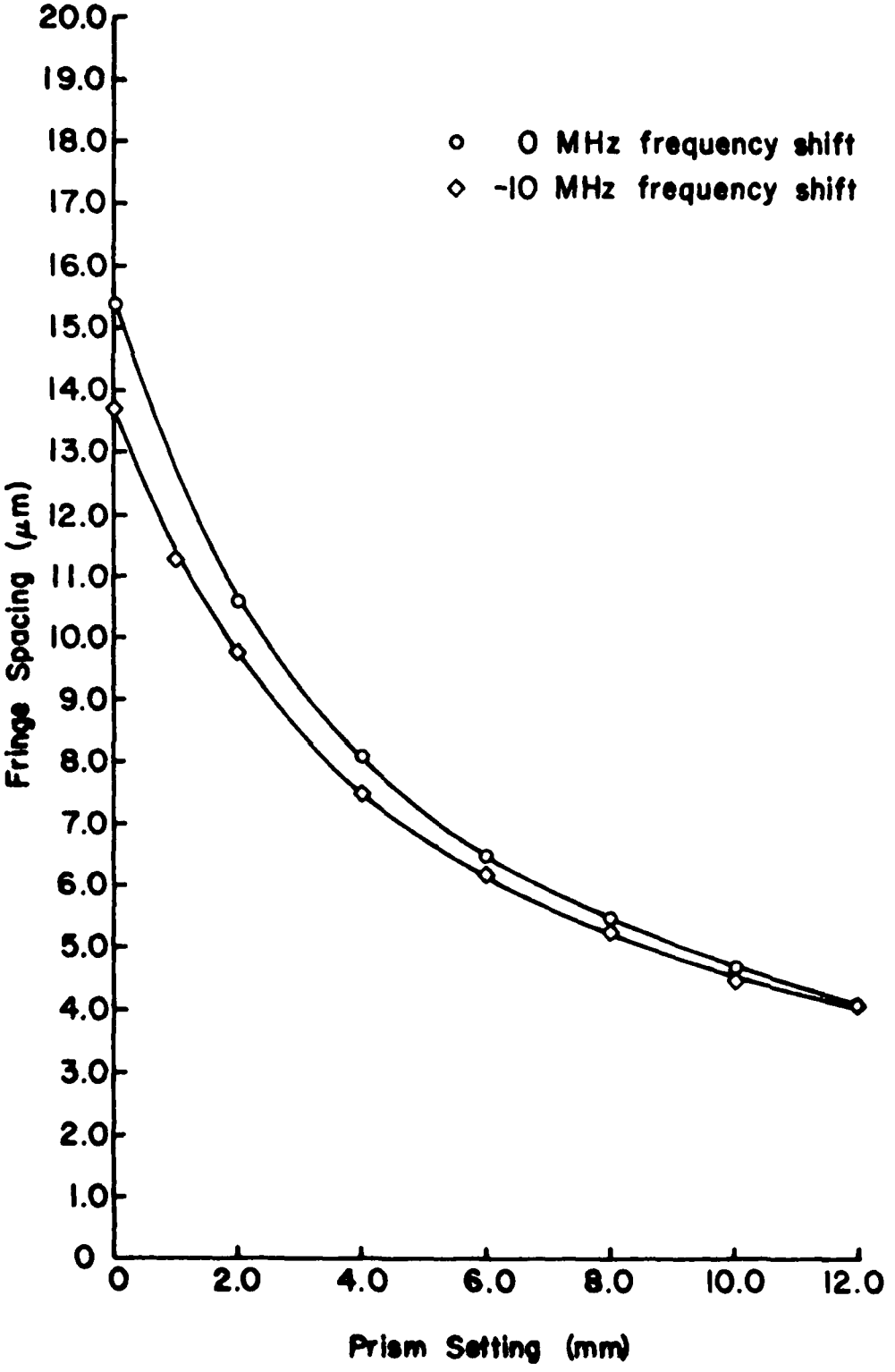

Figure 13. Fringe Spacing vs Prism Setting

SECTION III

EVALUATION OF BIAS ERRORS FROM ONE-DIMENSIONAL LDV MEASUREMENTS

1. Measurement of Turbulence Parameters

The problem of interest is how the bias errors which may exist in turbulent flow data can be extracted from single component LDV measurements. In this section a method for obtaining various turbulence quantities for one-dimensional measurements in the absence of bias is described. This will then be used as the basis for analytical models which indicate how the more important bias errors can be obtained from measured data.

We assume that the two input beams have an initial wavelength λ_o and propagate in directions $\hat{e}_1$ and $\hat{e}_2$. The collected radiation will heterodyne with the beat frequency ν given by

$$\nu = \frac{n\vec{V}}{\lambda_o} \cdot (\hat{e}_1 - \hat{e}_2) \tag{6}$$

where $\vec{V}$ is the velocity of the scattering particle. The dot product $\vec{V} \cdot (\hat{e}_1 - \hat{e}_2)$ defines the velocity component in the plane of the intersecting beams and in the $\hat{e}_n$ direction (see Figure 14). ν is independent of the scattering direction.

From vector algebra,

$$\hat{e}_1 - \hat{e}_2 = 2 \sin\left(\frac{\theta}{2}\right) \hat{e}_n \tag{7}$$

where θ is the angle between the incident beams.

For convenience we can align the LDV system so that the laboratory coordinates (x,y) are in the plane perpendicular to the $\hat{e}_t$ direction and the measured velocity component in the $\hat{e}_n$ direction is at any selected angle ϕ in the (x,y) plane (see Figures 14 and 15).

Then

$$\hat{e}_n = \cos\phi\ \hat{e}_x + \sin\phi\ \hat{e}_y \tag{8}$$

To support a turbulent flow model, let

$$\vec{V} = (\bar{u} + u')\hat{e}_x + (\bar{v} + v')\hat{e}_y + (\bar{w} + w')\hat{e}_z \tag{9}$$

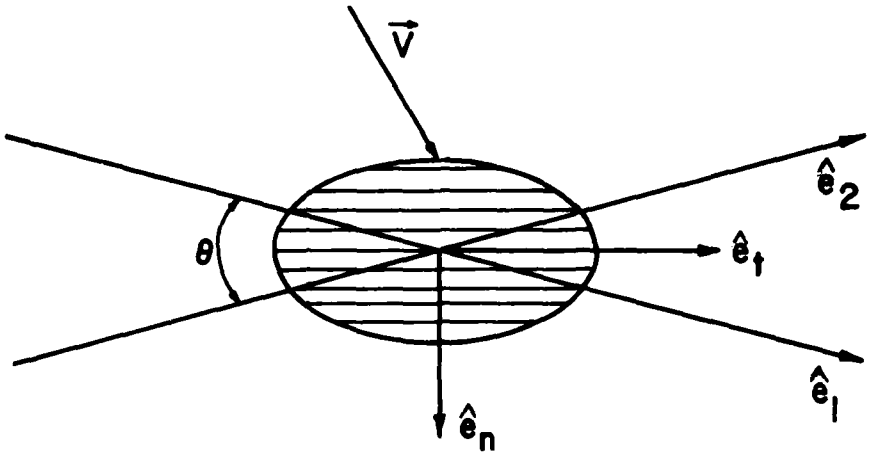

Figure 14. Probe Volume Geometry

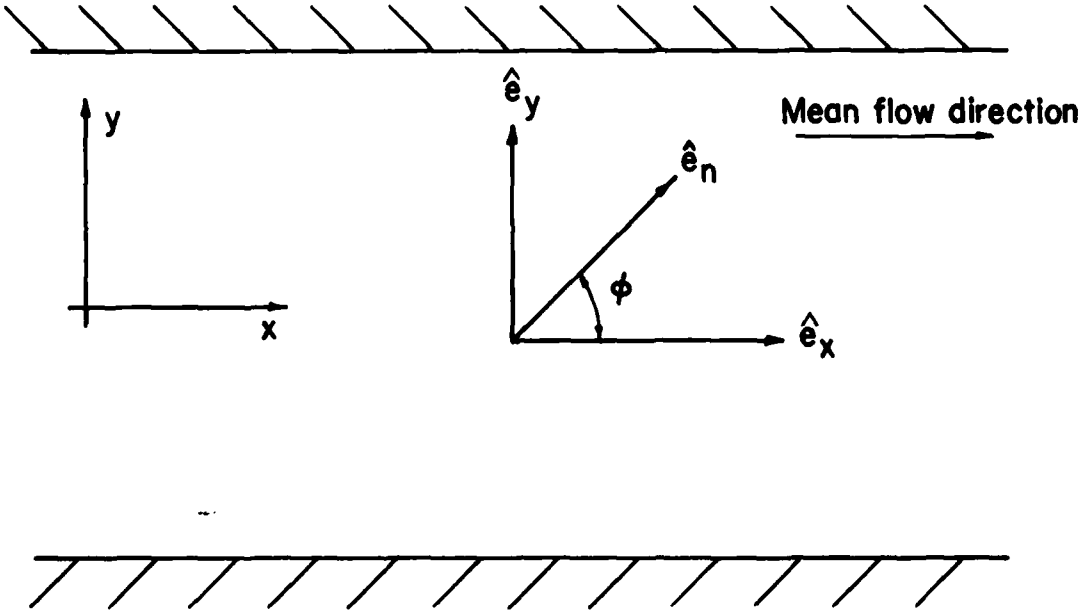

Figure 15. Flow System Geometry

and

$$\nu = \overline{\nu} + \nu' \tag{10}$$

where the bar indicates a time average quantity and the prime indicates an instantaneous fluctuation above or below the time average. Substituting Equation (8) into Equation (7) yields

$$\hat{e}_1 - \hat{e}_2 = 2 \sin\left(\frac{\theta}{2}\right) \cos\phi \, \hat{e}_x + 2 \sin\left(\frac{\theta}{2}\right) \sin\phi \, \hat{e}_y \tag{11}$$

Substituting Equations (9), (10), and (11) into Equation (6) yields

$$\overline{\nu} + \nu' = A[(\overline{u} + u') \cos\phi + (\overline{v} + v') \sin\phi] \tag{12}$$

where

$$A \equiv \frac{2n}{\lambda_o} \sin\left(\frac{\theta}{2}\right) \tag{13}$$

Time averaging Equation (12) yields

$$\overline{\nu} = A[\overline{u} \cos\phi + \overline{v} \sin\phi] \tag{14}$$

Squaring both sides of Equation (12), time averaging, and using Equation (14) to eliminate $\overline{\nu}^2$ yields

$$\overline{\nu'^2} = A^2[\overline{u'^2} \cos^2\phi + 2 \overline{u'v'} \cos\phi \sin\phi + \overline{v'^2} \sin^2\phi] \tag{15}$$

Equations (14) and (15) represent two equations in five unknowns, namely, $\overline{u}$, $\overline{v}$, $\overline{u'^2}$, $\overline{v'^2}$, and $\overline{u'v'}$. Logan [4,5] has pointed out that by measuring the

---

[4] Logan, S.E., "A Laser Velocimeter for Reynolds Stress and Other Turbulence Measurements," AIAA Journal, Vol. 10, No. 7, pp. 933-935, 1972.

[5] Logan, S.E., "A Laser Velocimeter Measurement of Reynolds Stress and Turbulence in Dilute Polymer Solutions," Ph.D. Thesis, California Institute of Technology, 1972.

time average Doppler frequency $\overline{\nu}$ and its variance $\overline{\nu'^2}$ at three different angles, these five quantities can be solved for explicitly. For example, measuring $\overline{\nu}$ and $\overline{\nu'^2}$ at $\phi = 0°$, $+45°$, and $-45°$ yields

$$\overline{u} = \overline{\nu}_o/A \tag{16}$$

$$\overline{u'^2} = \overline{\nu_o'^2}/A^2 \tag{17}$$

$$\overline{u} = (\overline{\nu}_{+45} + \overline{\nu}_{-45})/A\sqrt{2} \tag{18}$$

$$\overline{v} = (\overline{\nu}_{+45} - \overline{\nu}_{-45})/A\sqrt{2} \tag{19}$$

$$\overline{v'^2} = (\overline{\nu_{+45}'^2} + \overline{\nu_{-45}'^2} - \overline{\nu_o'^2})/A^2 \tag{20}$$

and

$$\overline{u'v'} = (\overline{\nu_{+45}'^2} - \overline{\nu_{-45}'^2})/2A^2 \tag{21}$$

Notice that Equations (16) and (18) are redundant for the determination of $\overline{u}$. In a later section we use this redundancy to determine bias error.

Measuring $\overline{\nu}$ and $\overline{\nu'^2}$ at $\phi = 0°$, $+30°$, and $+60°$ yields

$$\overline{u} = \overline{\nu}_o/A \tag{22}$$

$$\overline{u'^2} = \overline{\nu_o'^2}/A^2 \tag{23}$$

$$\overline{u} = (\sqrt{3}\,\overline{\nu}_{+30} - \overline{\nu}_{+60})/A \tag{24}$$

$$\overline{v} = (\sqrt{3}\,\overline{\nu}_{+60} - \overline{\nu}_{+30})/A \tag{25}$$

$$\overline{v'^2} = (2\overline{\nu_{+60}'^2} - 2\overline{\nu_{+30}'^2} + \overline{\nu_o'^2})/A^2 \tag{26}$$

and

$$\overline{u'v'} = (3\overline{\nu'^2_{+30}} - \overline{\nu'^2_{+60}} - 2\overline{\nu'^2_o})/A^2\sqrt{3} \tag{27}$$

Similarly, measuring $\overline{\nu}$ and $\overline{\nu'^2}$ at $\phi = 0°$, $+30°$, and $-30°$ yields

$$\overline{u} = \nu_o/A \tag{28}$$

$$\overline{u'^2} = \overline{\nu'^2_o}/A^2 \tag{29}$$

$$\overline{u} = (\overline{\nu}_{+30} + \overline{\nu}_{-30})/A\sqrt{3} \tag{30}$$

$$\overline{v} = (\overline{\nu}_{+30} - \overline{\nu}_{-30})/A \tag{31}$$

$$\overline{v'^2} = (2\overline{\nu'^2_{+30}} + 2\overline{\nu'^2_{-30}} - 3\overline{\nu'^2_o})/A^2 \tag{32}$$

and

$$\overline{u'v'} = (\overline{\nu'^2_{+30}} - \overline{\nu'^2_{-30}})/A^2\sqrt{3} \tag{33}$$

Many other combinations are also possible.

2. Directional Bias

Since the beat frequency ν is always positive, laser Doppler systems possess an inherent directional ambiguity bias which allows only the magnitude and not the absolute sense of the velocity vector to be determined. One effective means of resolving this bias is to introduce a known frequency shift (ν_s) into one of the incident intersecting beams. The shift should be substantially larger than the turbulent broadening of the signal. The Doppler shift due to the fluid motion is then added to (or subtracted from) this shift frequency giving the desired directional sensitivity.

For example, when beam 2 (Figure 14) is upshifted by a frequency ν_s the measured Doppler frequency ν is related to the velocity vector $\vec{V}$ by

$$\nu = \frac{n\vec{V}}{\lambda_o} \cdot (\hat{e}_1 - \hat{e}_2) + \nu_s \tag{34}$$

Thus

$$\nu - \nu_s = \overline{\nu} + \nu' - \nu_s = A[(\overline{u}+u')\cos\phi + (\overline{v}+v')\sin\phi] \tag{35}$$

Therefore, for a frequency shifted system the average and fluctuating velocity components are related to the measured (ν) and shift (ν_s) frequencies by

$$\overline{\nu} - \nu_s = A[\overline{u}\cos\phi + \overline{v}\sin\phi] \tag{36}$$

and

$$\overline{\nu'^2} = A^2[\overline{u'^2}\cos^2\phi + 2\overline{u'v'}\cos\phi\sin\phi + \overline{v'^2}\sin^2\phi] \tag{37}$$

Equation (36) is identical to Equation (14) if $\overline{\nu}$ is replaced by $\overline{\nu} - \nu_s$. Equations (15) and (37) do not contain the Doppler frequency and are inherently identical. Therefore, frequency shifting one of the incident intersecting beams to eliminate the directional ambiguity bias does not affect the analysis and Equations (16) through (33) are still valid.

3. Other Biases

In addition to directional bias individual realization LDV signals may be subject to biases from several other sources. Analysis indicates that the two most significant are the so called velocity bias and incomplete signal bias (See Reference [6]). It should be noted, however, that nonuniform seeding could also result in very significant bias errors.

McLaughlin and Tiederman [7] first conjectured that a velocity bias might exist in individual realization LDV measurements. They reasoned that in a uniformly seeded incompressible flow a greater volume of high velocity fluid (and therefore a larger number of seed particles) would pass through the probe volume than low velocity fluid. The natural conclusion is that an individual

---

[6] Thompson, H. and Flack, R., Jr., "An Application of Laser Velocimetry to the Interpretation of Turbulent Structure," Proceedings of the ISL/AGARD Workshop on Laser Anemometry, German-French Research Institute, Pfeifer, H. and Haertig, J., Editors, St.Louis, France, p. 189, 1976.

[7] McLaughlin, D. and Tiederman, W., "Biasing Correction for Individual Realization of Laser Anemometer Measurements in Turbulent Flows," The Physics of Fluids, Vol. 16, No. 12, p. 2082, December 1973.

realization counting system would count more fast particles than slow particles and, therefore, an ensemble (particle) averaged velocity would be higher than the true time averaged velocity.

It is important to realize that the concept of velocity bias has nothing whatever to do with the time required to process a signal. The idea that the processing time for a fast particle is less than that for a slow particle (because it takes less time to count a given number of cycles for a fast particle), and therefore more fast particles could be counted is an entirely separate consideration.

Incomplete signal bias occurs when a large proportion of the particles have significant transverse velocity components (perpendicular to $\hat{e}_n$), as would occur in a highly turbulent flow, and leave the probe volume before crossing enough fringes to give a valid signal. This would bias the measured mean velocity toward a high value, since these particles would have a small $\hat{e}_n$ component and this contribution to the measured mean velocity would be missed. Analysis indicates that incomplete signal bias may be very significant for velocity component measurements made at relatively high angles of the mean flow direction [6]. Incomplete signal bias is greatly reduced by frequency shifting whereas frequency shifting should have very little or no effect on velocity bias.

It should be noted that although bias errors have been predicted for many years, experimental studies have yielded conflicting results. In the case of velocity bias some investigations, such as [8], have confirmed a velocity bias, others have yielded inconclusive results [10]. Further discussion of previous studies is presented in the Appendix. In the next section we examine how definitive measurements of the velocity bias and other bias errors might be obtained.

4. Methods for Measuring Bias Errors

Consider a Doppler signal such as the one illustrated in Figure 16. The instantaneous frequency ν can be broken down into either a time average $\overline{\nu}$ plus a fluctuating part ν' or an ensemble average $\langle\nu\rangle$ plus a fluctuation about the ensemble average ν^*. Thus

---

[8] Quigley, M., and Tiederman, W., "Experimental Evaluation of Sampling Bias in Individual Realization Laser Anemometry," AIAA Journal, Vol. 15, No. 2, p. 266, February 1977.

[9] Giel, T. and Barnett, D., "Analytical and Experimental Study of Statistical Bias in Laser Velocimetry," Laser Velocimetry and Particle Sizing, Hemisphere Publishing Corporation, p. 86, 1979.

[10] Bogard, D. and Tiederman, W., "Experimental Evaluation of Sampling Bias in Naturally Seeded Flows," Laser Velocimetry and Particle Sizing, Hemisphere Publishing Corporation, p. 100, 1979.

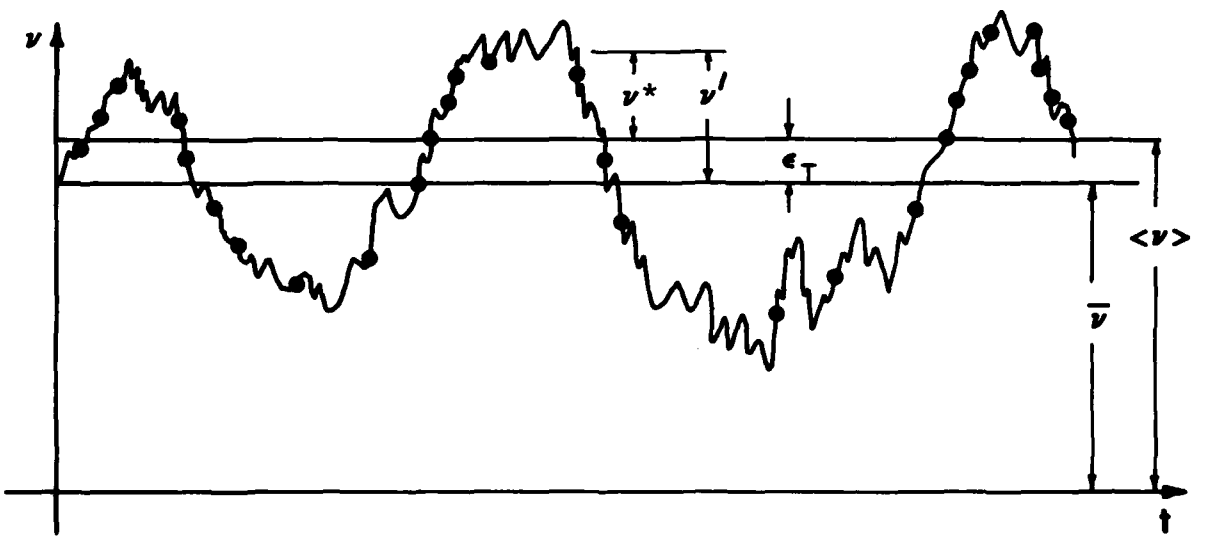

Figure 16. Time and Ensemble Averaged Doppler Signals

$$\nu = \bar{\nu} + \nu' = \langle \nu \rangle + \nu^* \tag{38}$$

Now if there is a bias in the signal such that the ensemble average frequency is greater than the time average frequency by an amount ε_T, then

$$\langle \nu \rangle - \bar{\nu} = \varepsilon_T \tag{39}$$

The bias ε_T is the total bias in the frequency measurement and is the sum of the velocity bias ε^*, the incomplete signal bias ε^{**}, and all other biases that may effect the system.

$$\varepsilon_T = \varepsilon^* + \varepsilon^{**} + \cdots \tag{40}$$

The objective is to formulate a scheme by which the individual bias errors can be obtained from LDV data. For the analysis it is assumed that the flow is incompressible, uniformly seeded, and that the only significant biases are velocity bias and incomplete signal bias. Two methods for making velocity bias measurements are proposed along with a method for making incomplete signal bias measurements. Certainly there are several other possibilities for making direct and indirect bias measurements including direct comparison with hot wire measurements. The methods proposed here are the first ones that will be attempted. Partial results are reported in Section IV.

4.1 Velocity Bias

In this section two methods are outlined for experimentally measuring the velocity bias. The first and simplest is to control the seed density and data sampling rate such that data sets approximating both ensemble averaged and time averaged measurements are obtained. For example, suppose that an individual realization LDV system has the capability of recording at a rate of 1000 Hz. Using that system and controlling the particle seeding so that only about 200 particles per second pass through the probe volume one would expect to record a velocity (component) for nearly every particle. The uncorrected average velocity would represent an ensemble (particle) average.

Now if the seeding density were increased so that say 20,000 particles per second passed through the probe volume while all other parameters remain the same, then the system would be limited by the data recording capability. Only the velocity of one particle in 20 (on the average) would be recorded. The data would be sampled at nearly equal time intervals and the uncorrected average velocity would tend toward a time averaged velocity. For this technique to work, care must be taken to eliminate other sources of possible bias.

The second method for measuring velocity bias is based on the analysis of Section III-1 and involves rotation of the optical system. The velocity

bias can be isolated by a proper frequency shift, since it is unaffected by the shift while the incomplete signal bias and most other biases are nearly eliminated by the shift. Therefore, in the frequency shifted mode the average velocity, $\bar{u}$, given by Equation (16) can be expressed in terms of the ensemble average frequency $\langle \nu_o \rangle$ and the velocity bias ε_o^* measured at $\phi = 0°$. Thus

$$\bar{u} = (\langle \nu_o \rangle - \varepsilon_o^*)/A \tag{41}$$

Similarly, Equation (18) becomes

$$\bar{u} = (\langle \nu_{+45} \rangle + \langle \nu_{-45} \rangle - \varepsilon_{+45}^* - \varepsilon_{-45}^*)/A\sqrt{2} \tag{42}$$

Combining Equations (41) and (42),

$$(\varepsilon_{+45}^* + \varepsilon_{-45}^* - \sqrt{2}\, \varepsilon_o^*) = \langle \nu_{+45} \rangle + \langle \nu_{-45} \rangle - \sqrt{2} \langle \nu_o \rangle \tag{43}$$

At this point we further postulate that the velocity bias is independent of the direction of measurement (i.e., independent of ϕ) such that

$$\varepsilon^* = \varepsilon_o^* = \varepsilon_{+45}^* = \varepsilon_{-45}^* \tag{44}$$

This assumption would appear to be true for isotropic turbulence, but may be of questionable validity for non-isotropic turbulence. If it is true, then

$$\varepsilon^* = \frac{\langle \nu_{+45} \rangle + \langle \nu_{-45} \rangle - \sqrt{2} \langle \nu_o \rangle}{2 - \sqrt{2}} \tag{45}$$

In a similar manner the average velocities given by Equations (22) and (24) can be used to obtain the result for measurements at $\phi = 0°$, $+30°$, and $+60°$.

$$\varepsilon^* = \frac{\langle \nu_o \rangle + \langle \nu_{+60} \rangle - \sqrt{3} \langle \nu_{+30} \rangle}{2 - \sqrt{3}} \tag{46}$$

For the ϕ = 0, +30, and -30 degree set of measurements

$$\varepsilon^* = \frac{\langle \nu_{+30} \rangle + \langle \nu_{-30} \rangle - \sqrt{3} \langle \nu_0 \rangle}{2 - \sqrt{3}} \tag{47}$$

Many other combinations are also possible.

It is interesting to note that under the above assumptions and when angular measurements of + and - the same angles are used, the ensemble averages give the correct value of the average velocity $\bar{v}$. That is, from Equation (19),

$$\bar{v} = (\langle \nu_{+45} \rangle - \langle \nu_{-45} \rangle)/A\sqrt{2} \tag{48}$$

or from Equation (31),

$$\bar{v} = (\langle \nu_{+30} \rangle - \langle \nu_{-30} \rangle)/A \tag{49}$$

4.2 Incomplete Signal Bias

Measurement of the incomplete signal bias (ε^{**}) is necessarily more complex than measurement of the velocity bias, since it is not possible to isolate the incomplete signal bias and it must therefore be considered along with the velocity bias. From the analysis in Reference [6] we expect that unshifted measurements in a highly turbulent flow at relatively large measuring angles ϕ will show a rather large incomplete signal bias. Thus by assuming $\varepsilon^{**}_{+45} = \varepsilon^{**}_{-45}$, and $\varepsilon^{**}_0 \simeq 0$, the average velocity measurements of Equations (16) and (18) can be combined similar to the procedure in the previous section for the velocity bias to give

$$\varepsilon^{**}_{\pm 45} = \frac{\langle \nu_{+45} \rangle + \langle \nu_{-45} \rangle - \sqrt{2} \langle \nu_0 \rangle}{2} - \frac{2 - \sqrt{2}}{2} \varepsilon^* \tag{50}$$

where ε^* is the velocity bias calculated in Equation (45) from frequency shifted measurements.

Similarly, from the unshifted measurements at ϕ = 0, +30, and -30 degrees

$$\varepsilon^{**}_{\pm 30} = \frac{\langle \nu_{+30} \rangle + \langle \nu_{-30} \rangle - \sqrt{3} \langle \nu_0 \rangle}{2} - \frac{2 - \sqrt{3}}{2} \varepsilon^* \qquad (51)$$

where ε^* is the velocity bias calculated in Equation (47) from frequency shifted measurements.

SECTION IV

EXPERIMENTAL VERIFICATION OF VELOCITY BIAS

1. Methodology

In Section III-4.1 two methods were described for experimentally measuring a velocity bias. The first and simplest involves measurements at variable seeding rates to obtain both ensemble (particle) averaged data and time averaged data. The second method requires rotation of the optics to make frequency shifted measurements at several angles to the flow. Preliminary results using the first method have been obtained and are reported here.

Velocity bias was investigated by looking at one point in the flow and collecting a fixed number of data points (on the order of 4500) at each of several data rates controlled by the particle seeding density. Seeding density was varied by running the TSI model 3076 atomizer at a constant setting and bypassing a selected portion of the output. This allowed the particle data rate (as monitored on the TSI Model 1980 signal processor) to be accurately set without disturbing the atomizer. The TSI Model 3072 evaporation-condensation unit was employed to insure a nearly monodisperse aerosol of about 1 μm diameter. DOP was used as the seeding agent.

With the optics properly adjusted and the processor operating in the n-burst mode and counting 16 cycles per burst, the maximum data rate is approximately 20000 points per second. The minimum data rate depends on the amount of natural seed in the air and usually runs about 50 to 100 points per second.

When the TSI processor has a data point ready, it sends a data ready pulse to the micro-processor. When the micro-processor receives the pulse, it returns a data inhibit pulse to the TSI processor which causes it to hold that point until the micro-processor can record the point and process it. Once the point is sampled, the micro-processor removes the data inhibit, waits for another data ready pulse, and the process continues. The computer speed is variable, but at the present time its maximum speed is about 2000 points per second. The rate at which velocities are sampled and recorded is dependent on the slowest unit in the system.

An ensemble average will approximate a time average if the samples are taken at equal or nearly equal increments of time. It is possible to obtain a close approximation to sampling at equal increments of time by paying careful attention to the data rate and computer speed. Consider the case where the data rate is at its maximum of 20000 samples per second and the computer speed is at its maximum of 2000 samples per second. Thus, the sampling speed is controlled by the computer which is the slower of the two devices. When the computer is ready for a sample, the TSI processor will have a point ready in a very short time due to the high data rate. As a result, the computer will be sampling at very close to 2000 points per second at nearly equal time intervals.

Conversely, if the computer is operating at 2000 samples per second and the data rate is 200 samples per second, the TSI processor controls the data rate. The computer will sample every point the TSI processor computes and the increment between samples will depend on the arrival time between particles. As a result, the ensemble average will be a biased approximation to the time average. The amount of bias will be a function of the computer speed and the data rate.

Velocity bias is dependent on turbulence intensity. Measurements in laminar flow should yield no bias. As turbulence intensity increases, velocity bias should also increase. Measurements for this investigation were made in both low and high turbulence flows. The flow system used is shown in Figure 17. The low turbulence region is in the center of the tunnel, upstream of the step. Downstream of the step measurements were made at the six locations indicated in Figure 17. The results are presented in the following section.

2. Velocity Bias Measurements

Figure 18 shows the measured mean velocity at several different seeding densities at a point upstream of the step in a low turbulence region. The data are the average axial component of velocity and were taken with no frequency shift. The data rate is the rate at which the TSI processor was operating and was controlled by changing the seeding density as noted above. All other parameters remained constant. The maximum rate at which the microcomputer receives the processes data is about 2000 samples per second. Therefore, in interpreting the measured results the data at 250 samples per second was being stored as fast as it was being processed and the average velocity is an ensemble (particle) average. On the other hand the data at 10,000 samples per second was being processed so fast that the computer could only sample about one point in 5 resulting in essentially a time average sampling of the data. The points between are a mixture of time and ensemble averages. Figure 18 shows that for a low turbulence intensity (about 1%) the average velocities are independent of the data rate. Thus the ensemble average is equal to the time average. This is the expected result.

Figure 19 is a plot of the calculated turbulence intensity corresponding to the data in Figure 18. The histograms are made up of about 4500 measurements each. The few points that were outside a 3σ band were discarded. The one percent turbulence level is about what would be expected in the flow system, since no effort was made to attain extremely low turbulence levels upstream of the step.

A region of much higher turbulence intensity occurs in a shear layer which develops downstream of the step. Measurements were made at various downstream locations in this shear layer at the level of the step as indicated in Figure 17. Plots of this data are shown in Figures 20 through 31. The X location indicated on these plots refers to the downstream position of the measurement from the face of the step. All measurements were made at the center of the tunnel with zero frequency shift.

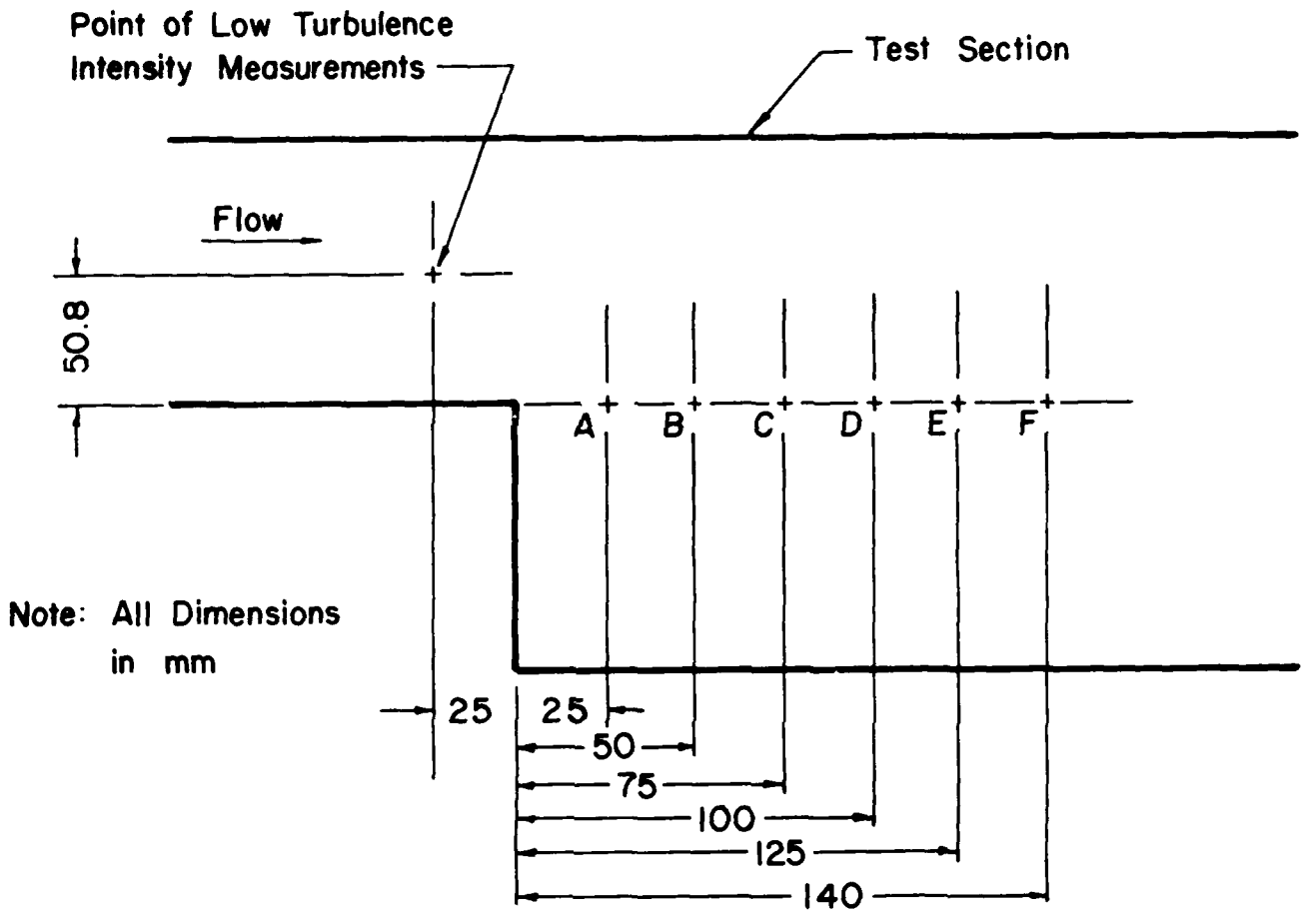

Figure 17. Measurement Locations in Test Section

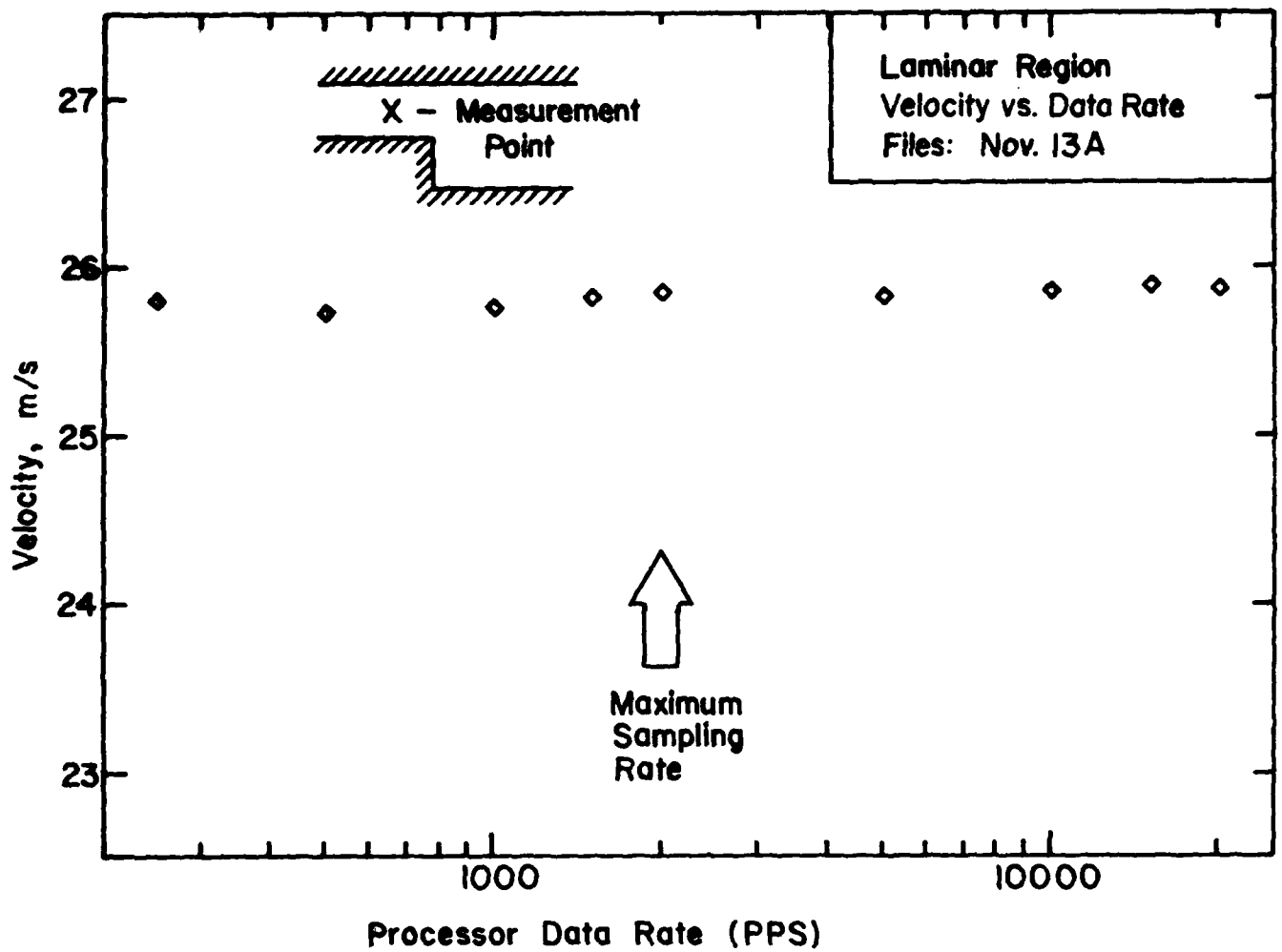

Figure 18. Velocity vs Data Rate in Laminar Region

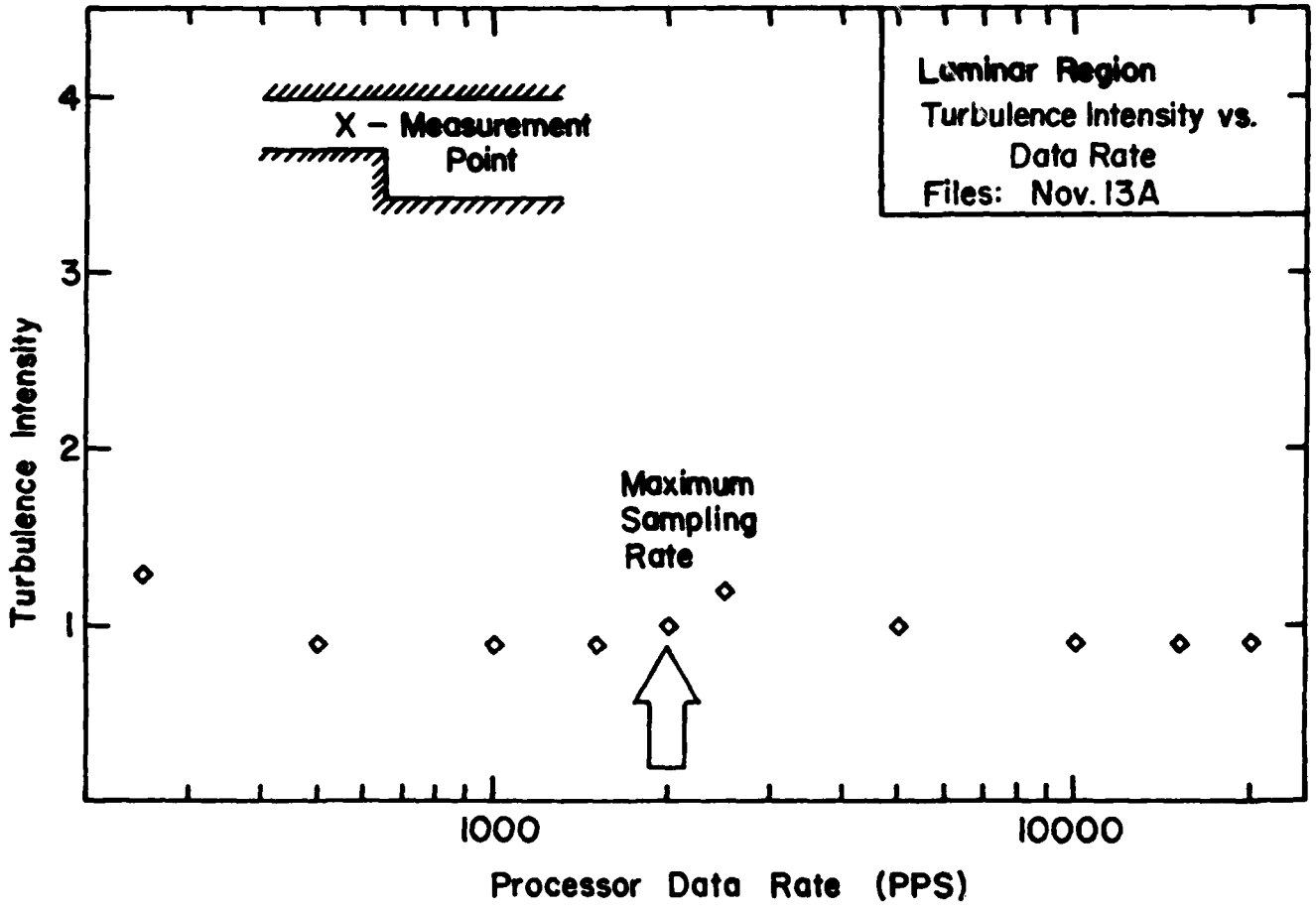

Figure 19. Turbulence Intensity vs Data Rate in Laminar Region

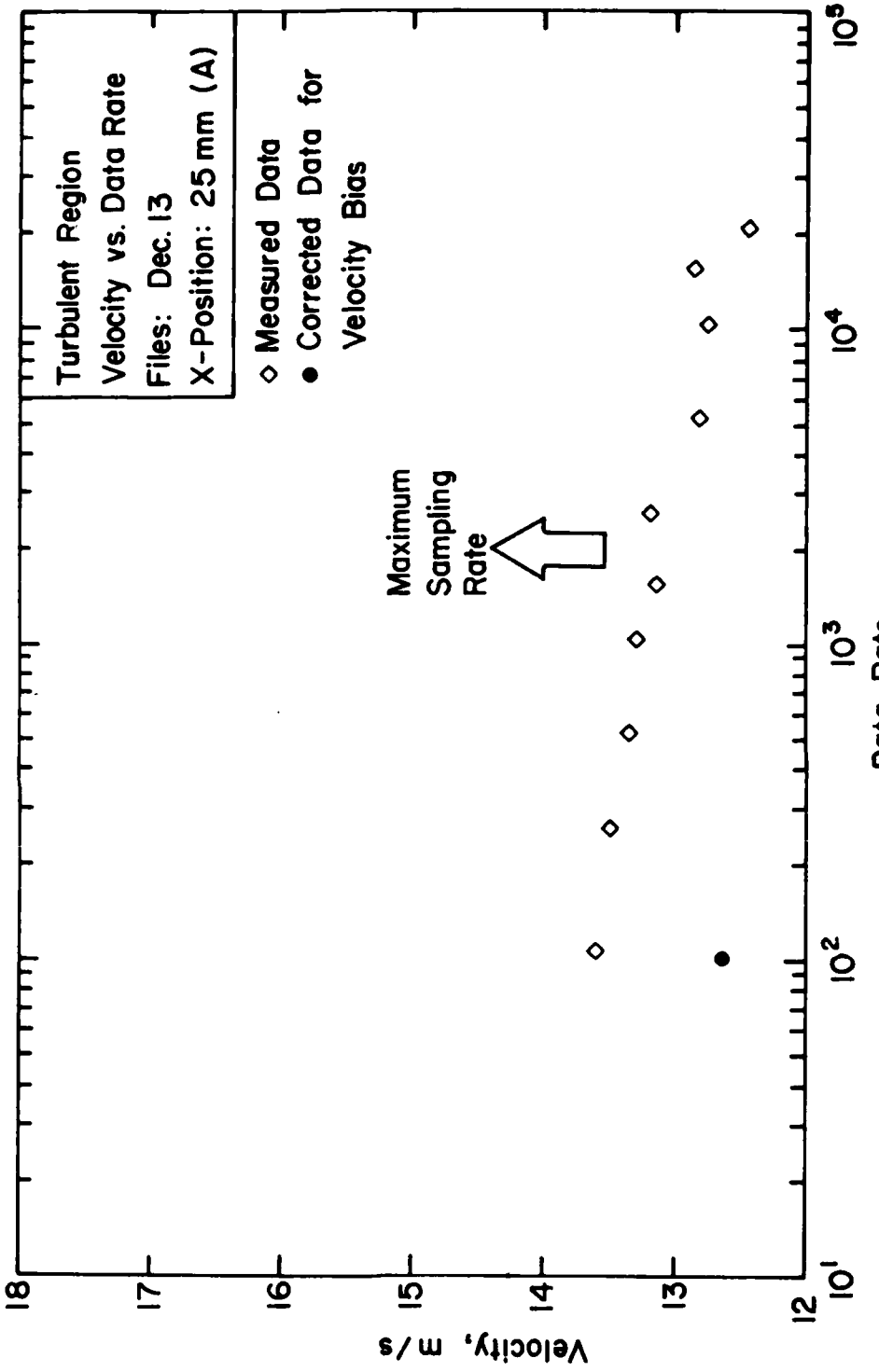

Figure 20. Velocity vs Data Rate at Location A

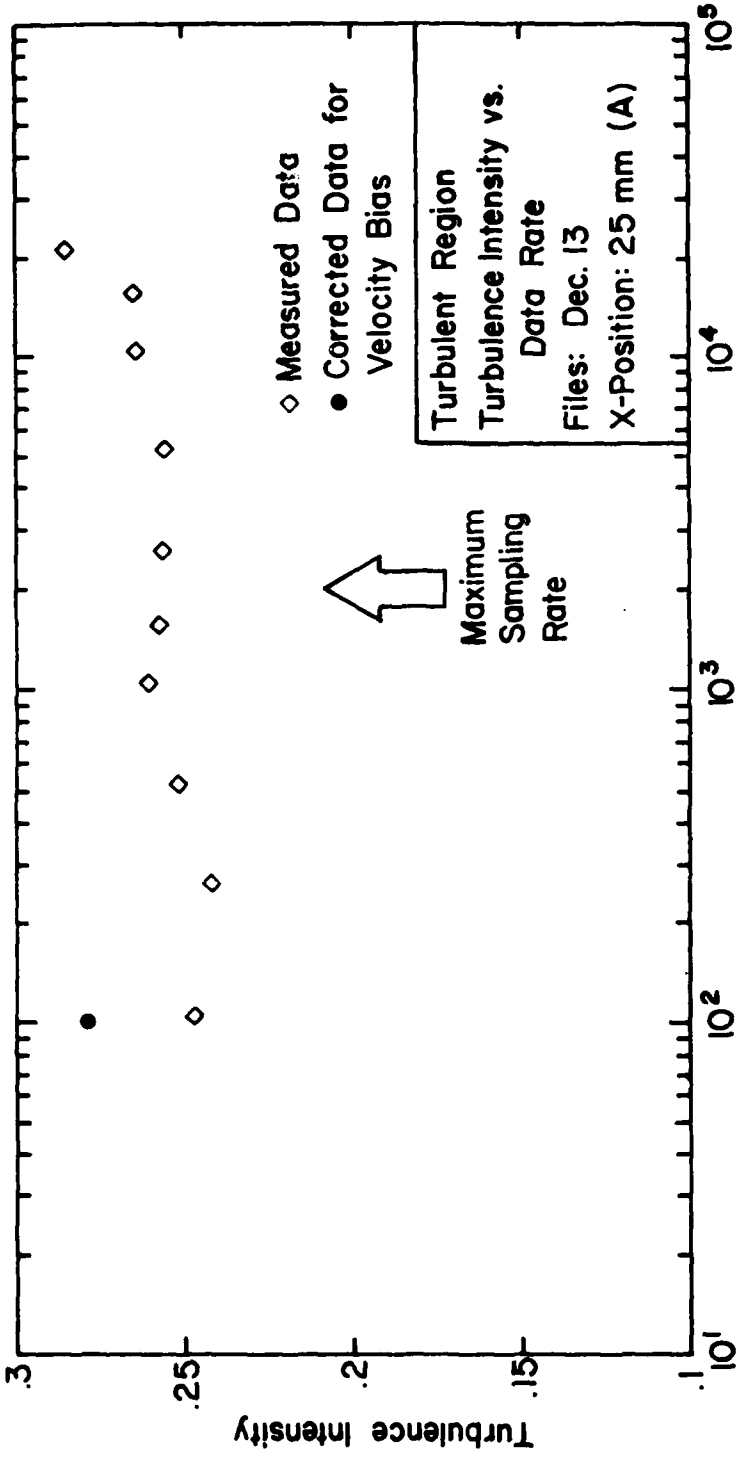

Figure 21. Turbulence Intensity vs Data Rate at Location A

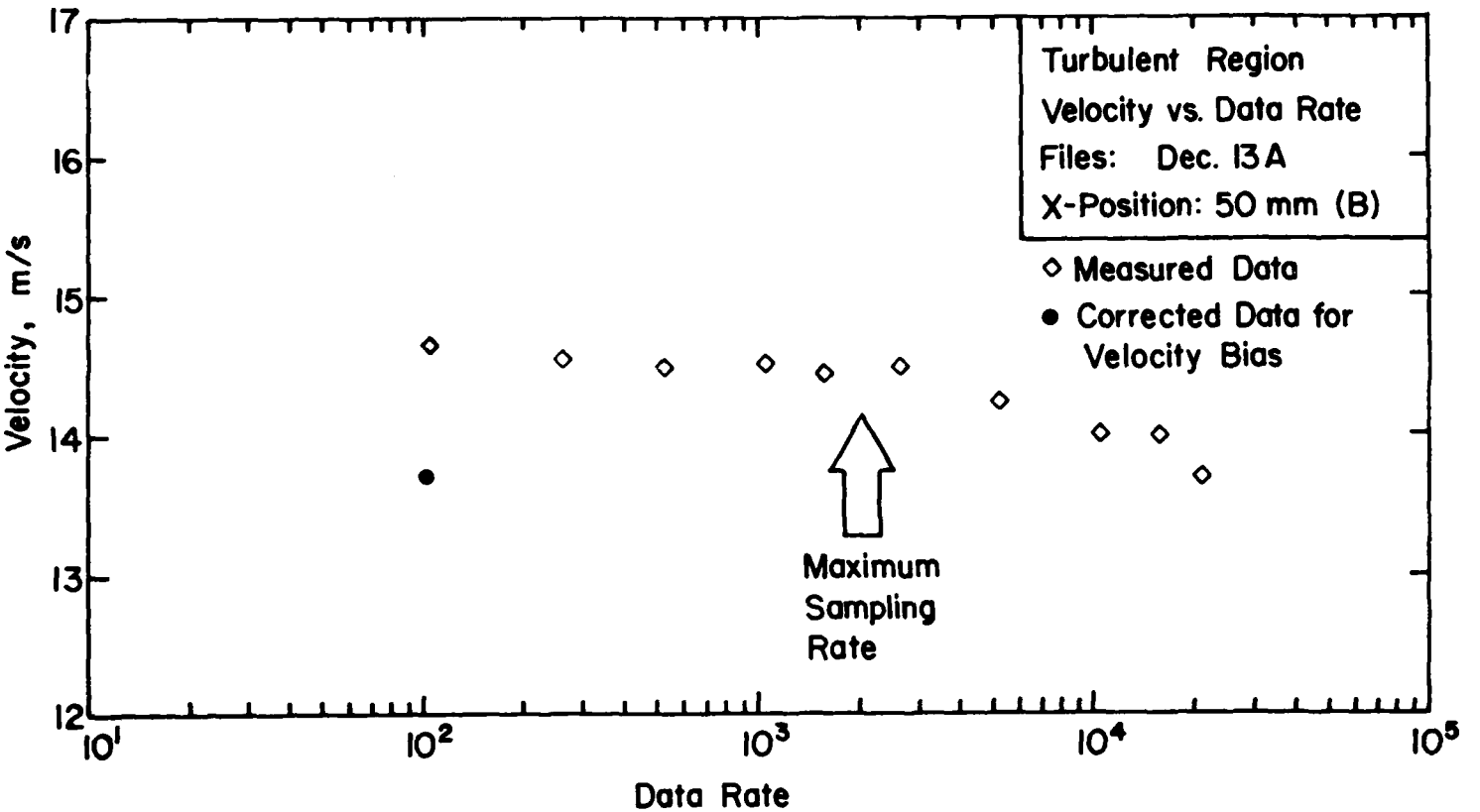

Figure 22. Velocity vs Data Rate at Location B

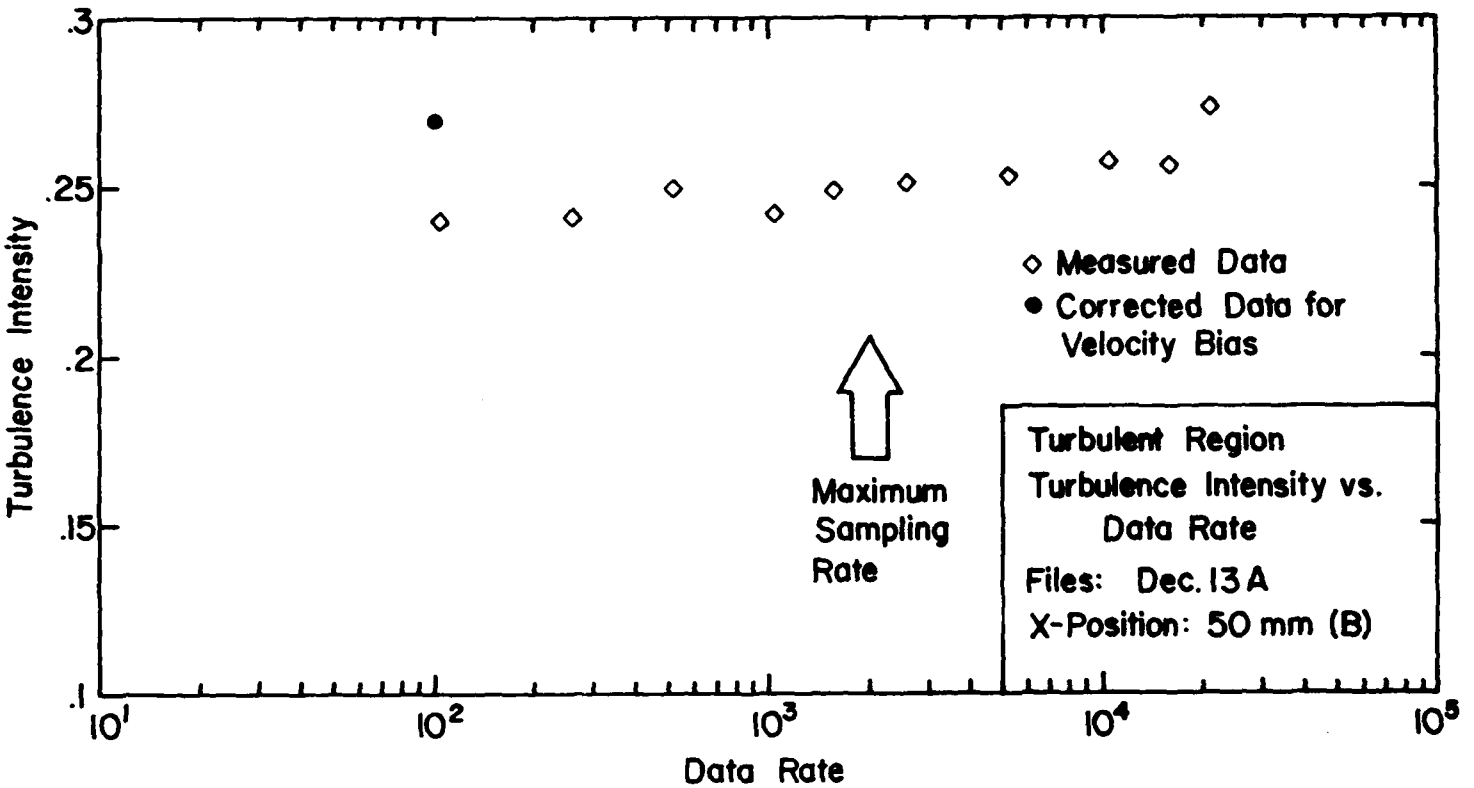

Figure 23. Turbulence Intensity vs Data Rate at Location B

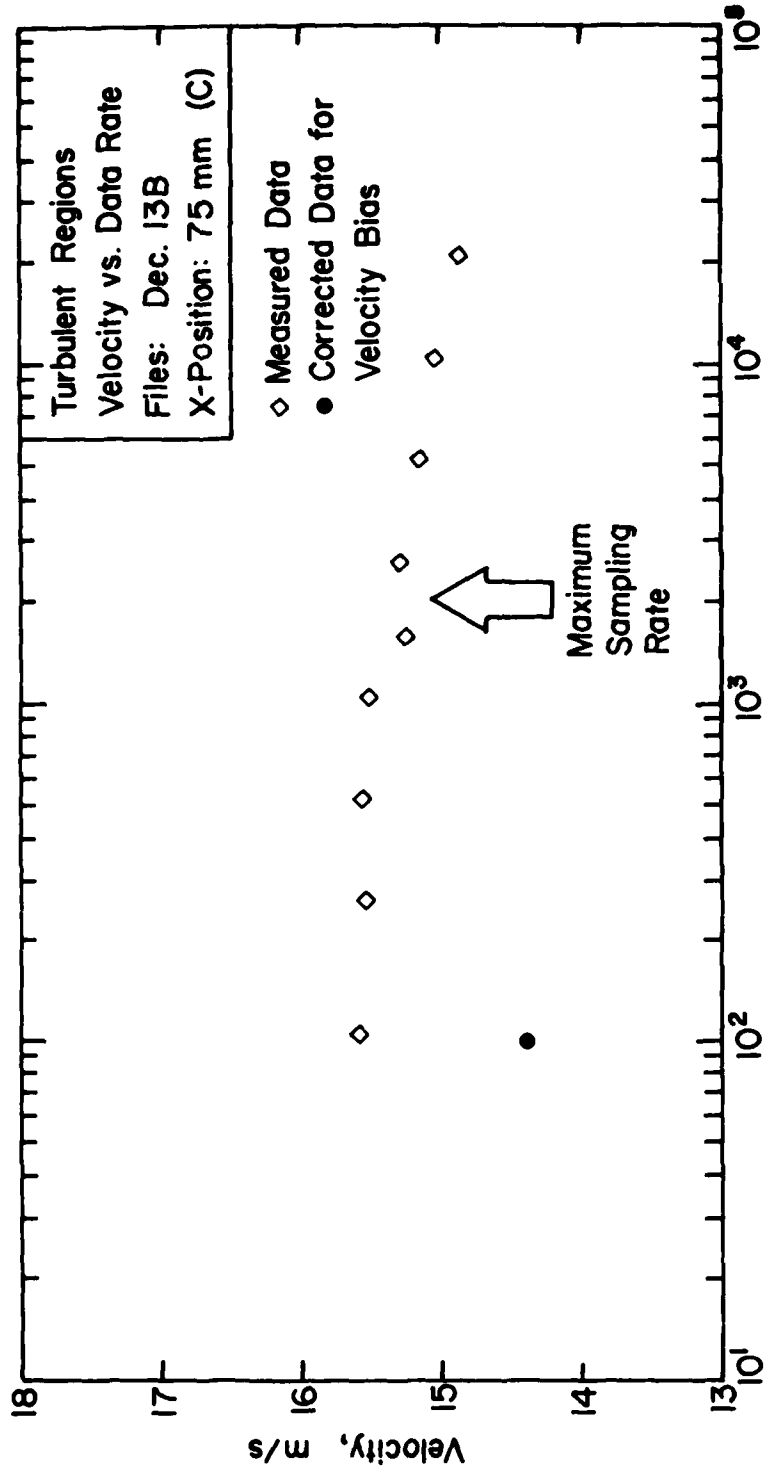

Figure 24. Velocity vs Data Rate a Location C

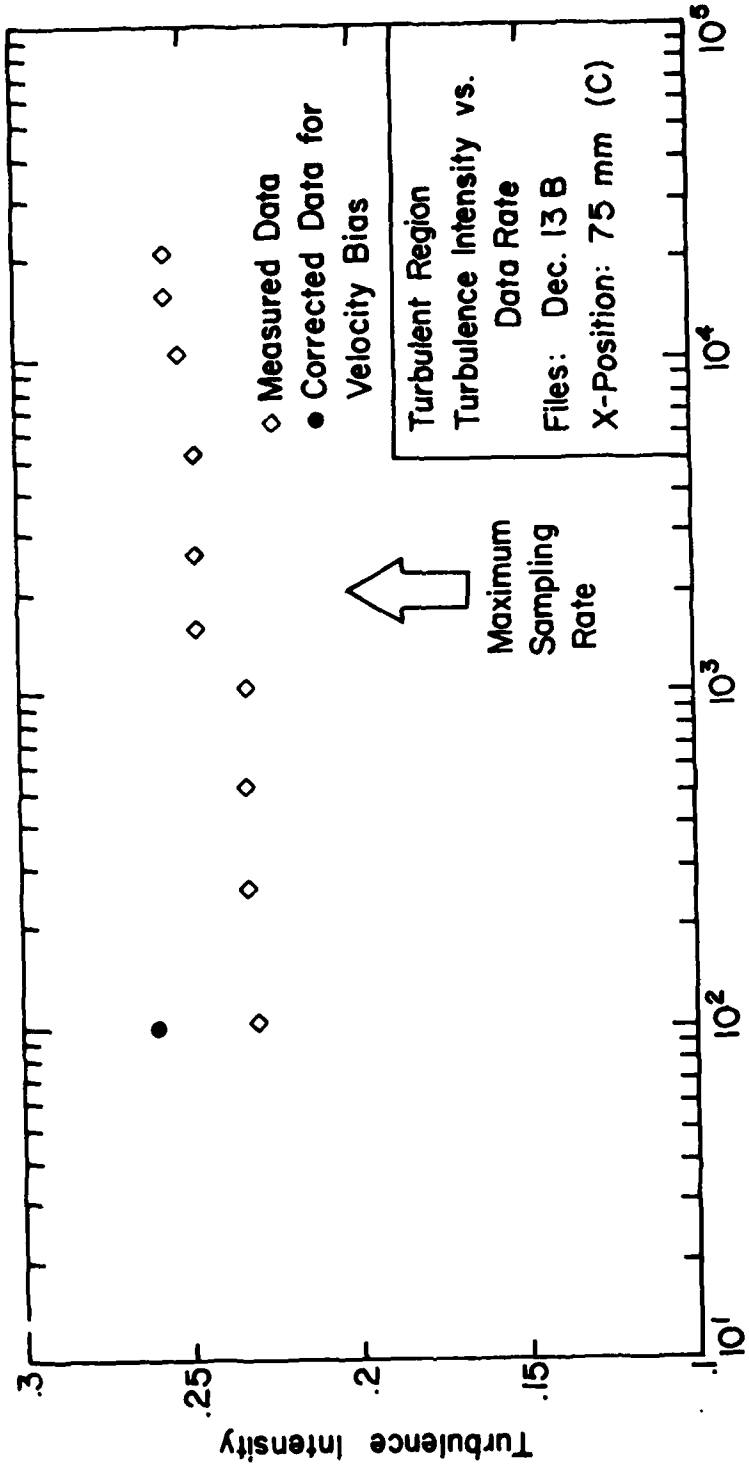

Figure 25. Turbulence Intensity vs Data Rate at Location C

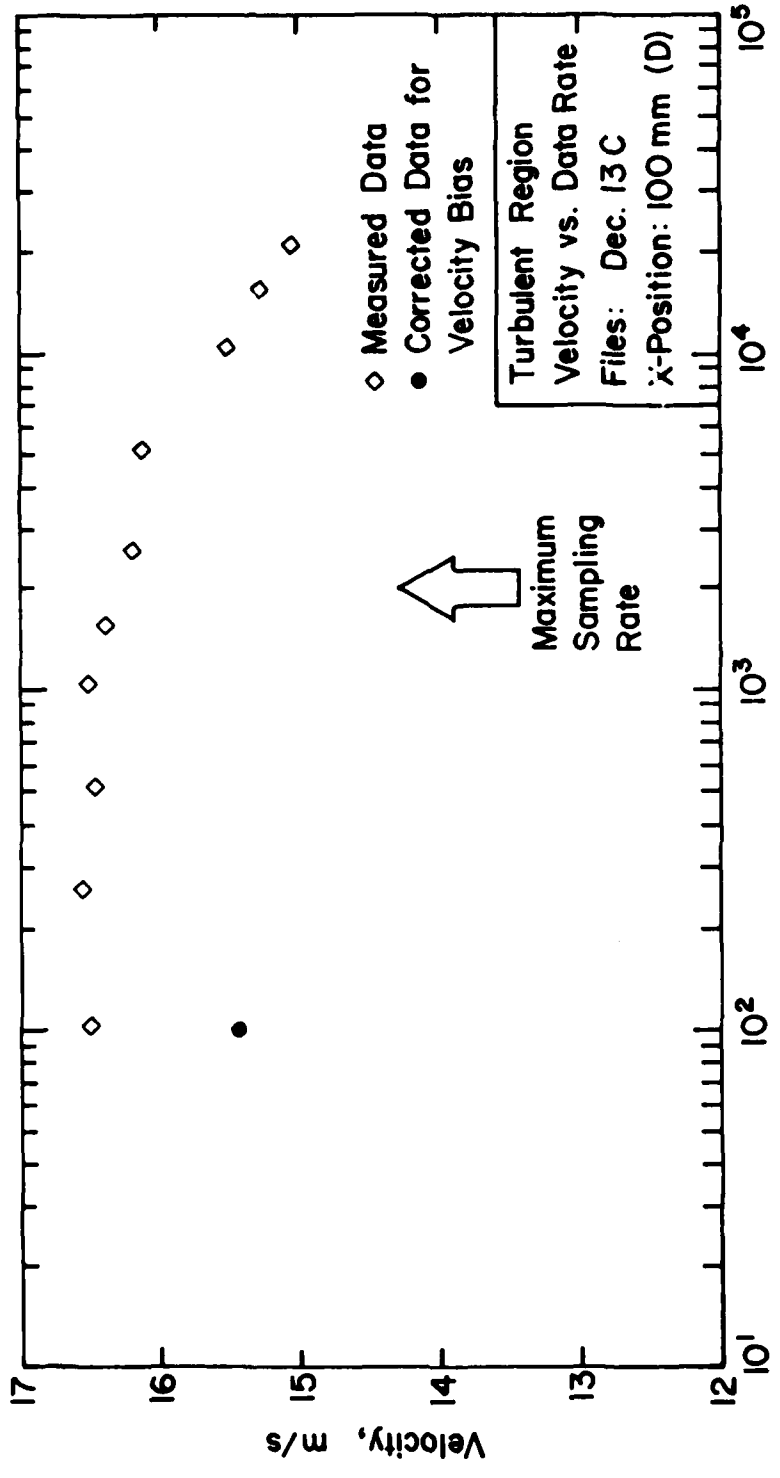

Figure 26. Velocity vs Data Rate at Location D

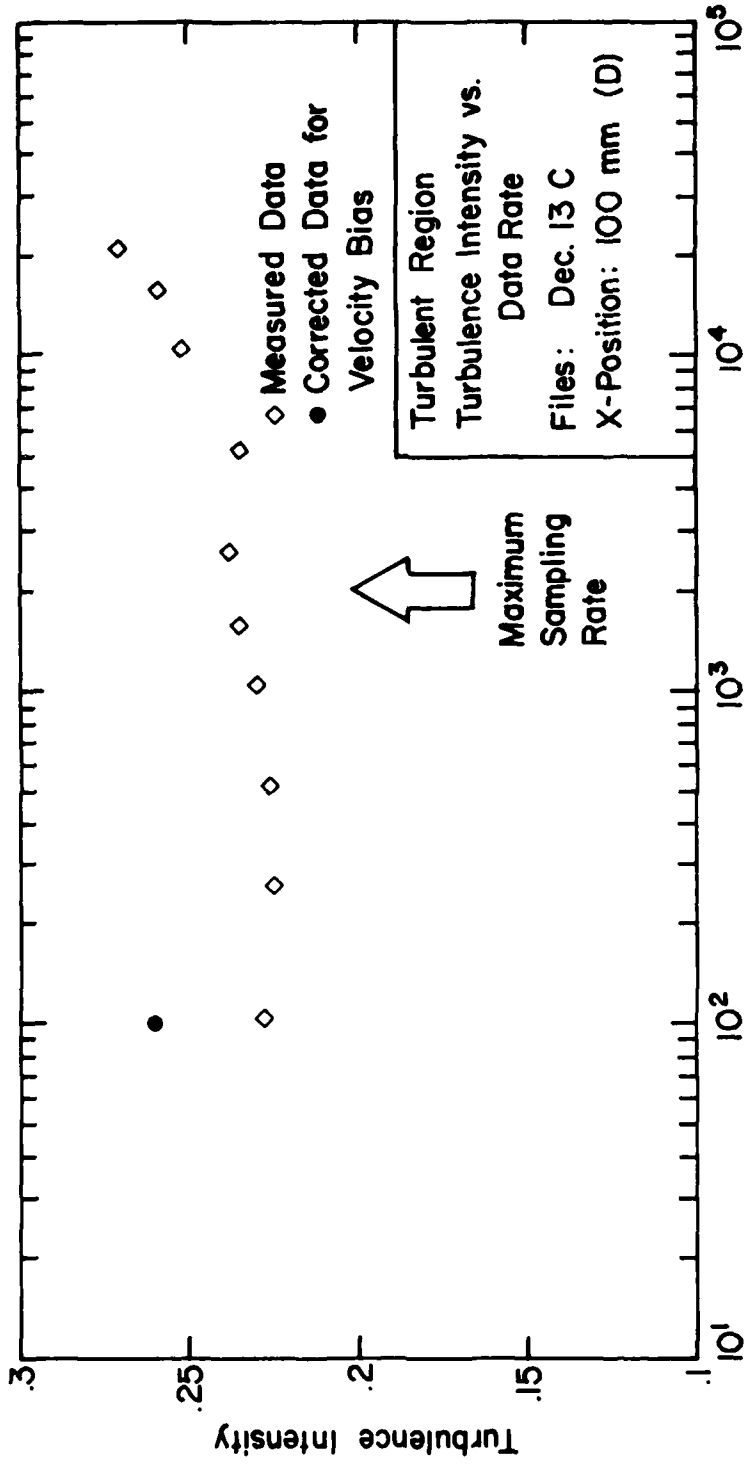

Figure 27. Turbulence Intensity vs Data Rate at Location D

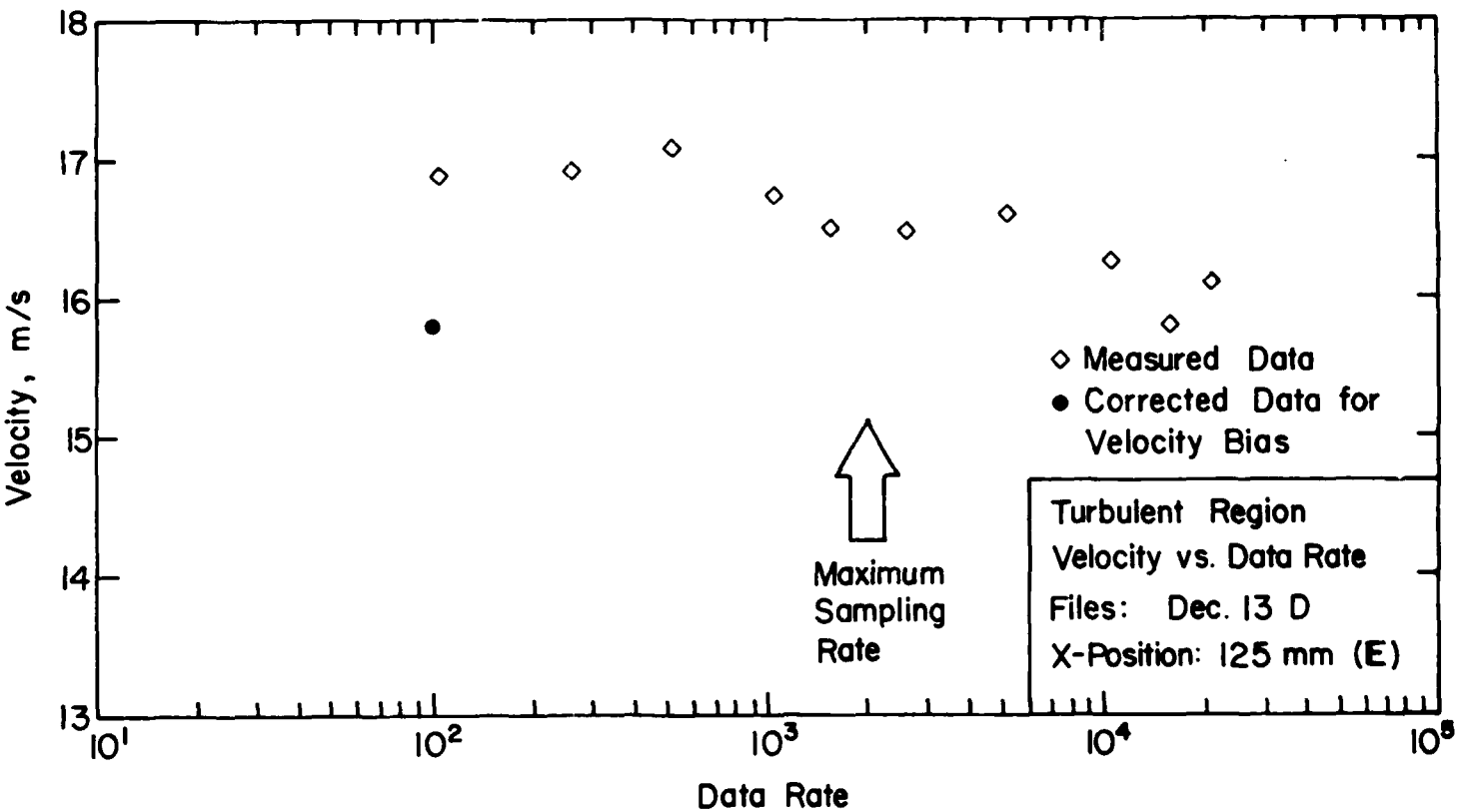

Figure 28. Velocity vs Data Rate at Location E

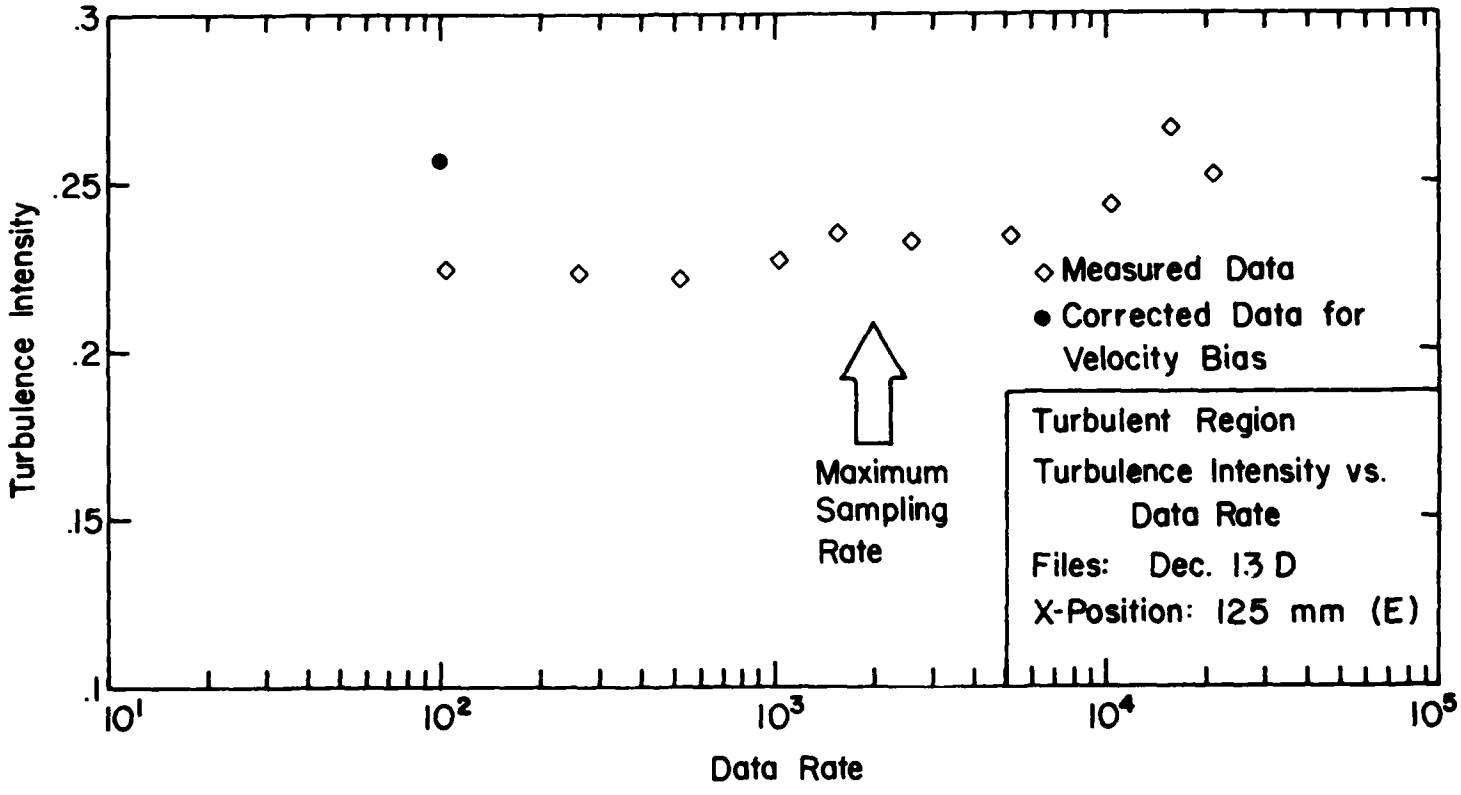

Figure 29. Turbulence Intensity vs Data Rate at Location E

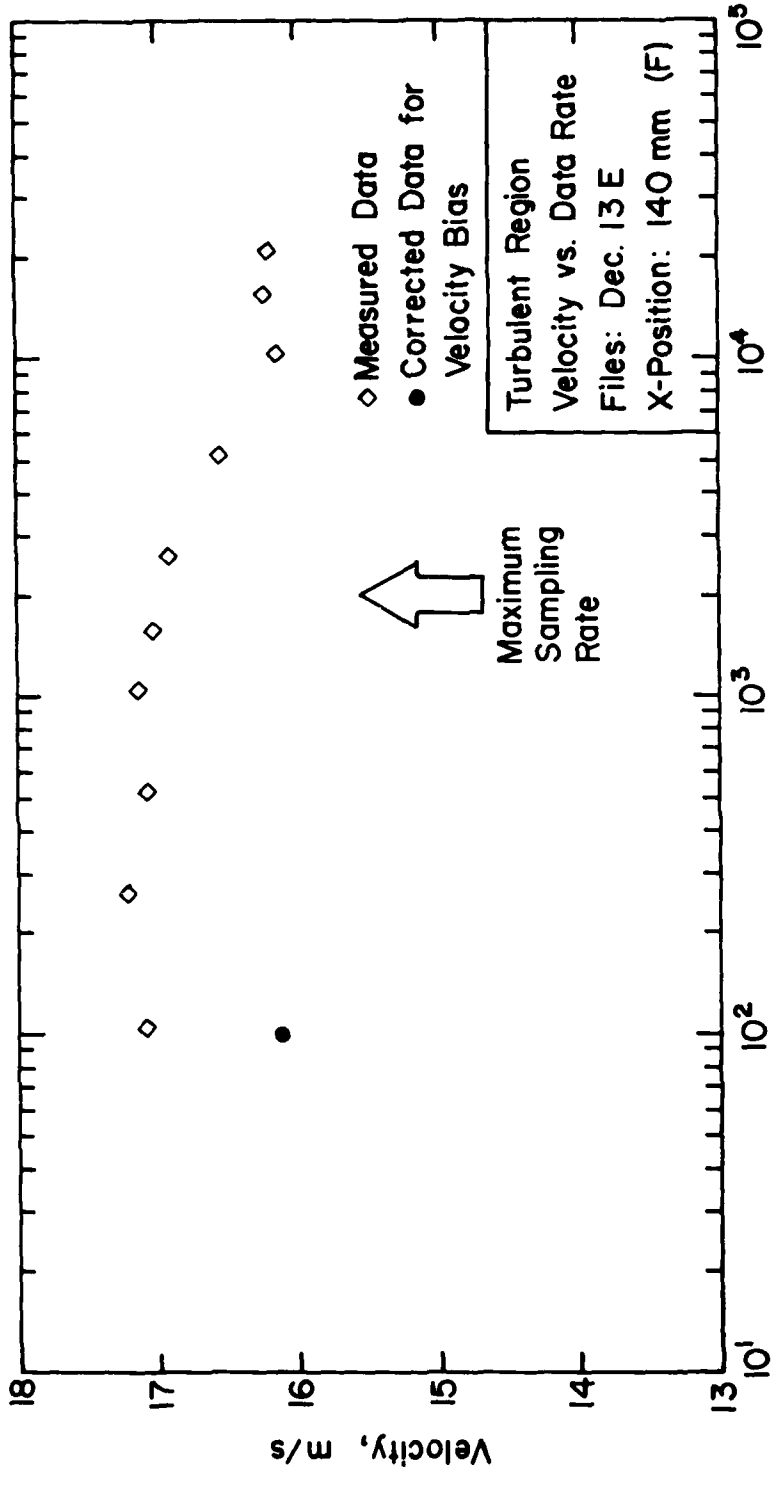

Figure 30. Velocity vs Data Rate at Location F

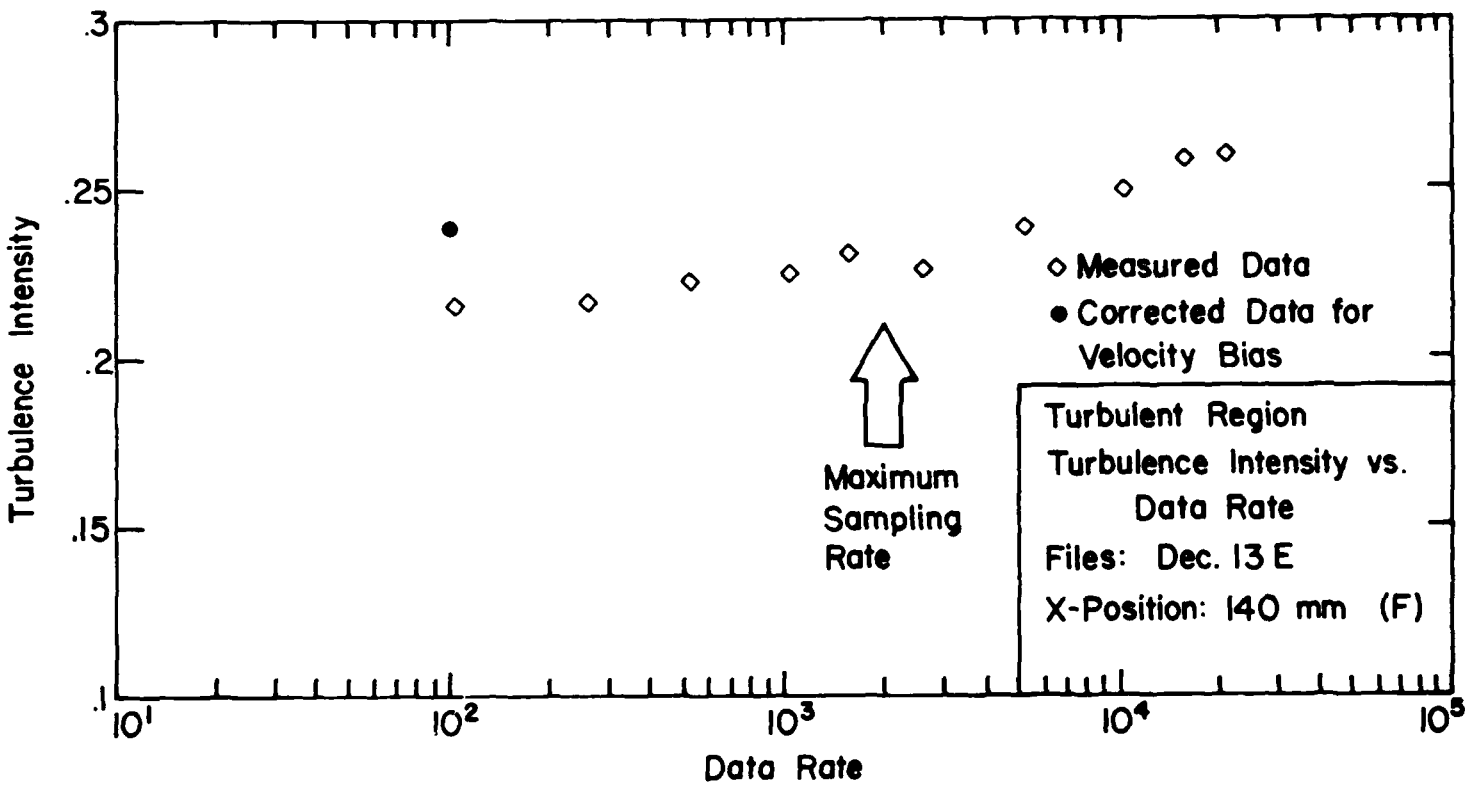

Figure 31. Turbulence Intensity vs Data Rate at Location F

Examination of these plots reveals a trend of decreasing mean velocity and increasing turbulence intensity with increasing data rate. In view of the earlier discussion on velocity bias one would expect a nearly constant mean velocity at data rates well below the computer speed. As the data rate approaches the computer speed, the velocity should decrease. At data rates significantly higher than the computer speed, one would expect a nearly constant mean velocity, but somewhat below the initial measurements. Plots for turbulence intensity should have an inverted behavior. Figures 20 through 31 have the proper trends. However, not all of them show the two constant velocity regions mentioned above. At low data rates a flat region is generally observed, but not always at high data rates. Measurements would need to be made at higher rates than we can presently attain to completely define the behavior.

Included on each plot in Figures 20 through 31 is one point (indicated by a solid circle) at the lowest data rate which represents the corrected average velocity or turbulence intensity using McLaughlin and Tiederman's one dimensional velocity weighting. In most cases, this value corresponds rather well with the supposed unbiased time average measurement at the highest data rate. Although these results seem to clearly indicate the existence of a velocity bias with a magnitude nearly equal to that predicted, this conclusion can only be preliminary at this point. This is because of problems we have encountered in measurements of this type made under different conditions. For example, Figure 32 shows three sets of data taken with different combinations of computer sampling rate and processor setting (cycles per burst). The general trend is the same, but there are disturbing ambiguities in the data taken at a sampling rate of 2000 Hz with the processor set to measure 16 cycles. We have also found discrepancies between frequency shifted data and unshifted data and between data taken when the processor was operating in the n-burst (fixed number of cycles per burst) and the total burst modes. It is not clear whether these effects are due to a processor defect or a problem in our computer system. We are studying this to determine the source of the variations observed.

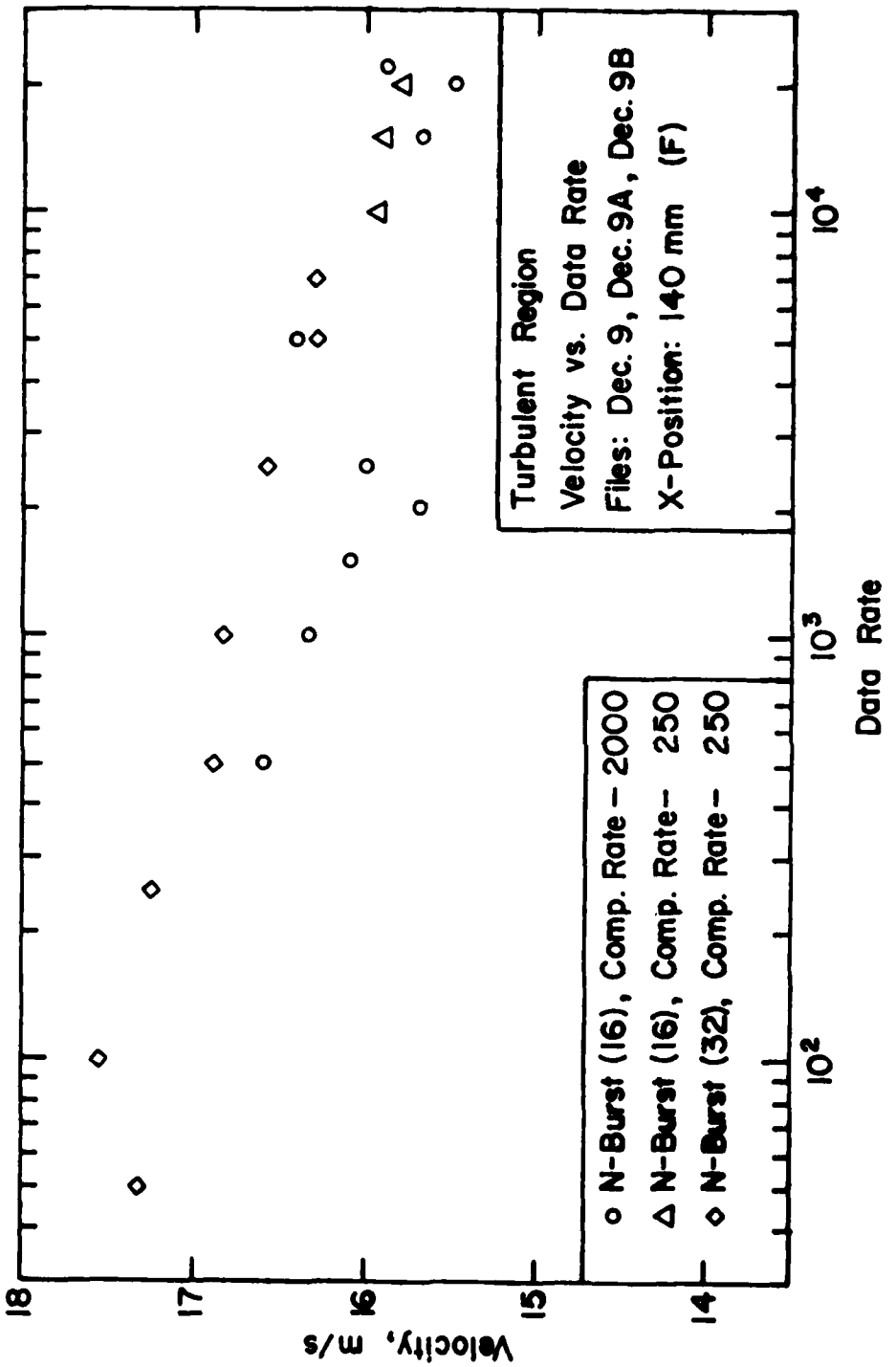

Figure 32. Velocity vs Data Rate at Location F for Various Computer Speeds and Cycles per Burst

SECTION V

FLOW OVER A REARWARD-FACING STEP

The flow over a rearward-facing step (which simulates a dump combustor) has been the subject of many investigations in the literature. Only in a few cases have experimental flow field data been compared to analytical solutions. This is due mainly to the difficulty involved in modeling the governing differential equations numerically. Experimental results for this type of flow can serve as a check on the analytical solution and as a guide to its validity. It is the purpose of this chapter to provide preliminary results of the present analytical and experimental work. The governing equations and the results of a detailed computer prediction for the flow over a step which models our two-dimensional flow facility are presented. In addition, static wall pressure measurements are compared with similar measurements of other researchers.

1. Analytical Model

To mathematically model steady, two-dimensional, turbulent flows with recirculation requires knowledge of the physical laws governing the transport, creation, and destruction of turbulence. With this knowledge, cast in mathematical form, a scheme for solving the resultant differential equations can be written into a computer program.

Recirculating flows, such as those found in a dump combustor, pose two major problems for the computational modeler: (1) there is no single predominant direction of flow; that is, reverse flow is present, and (2) turbulence dissipation is important in all coordinate directions. Hence, the flow in a dump combustor (cold flow) is governed by the elliptic Navier-Stokes differential equations. These time-averaged equations contain unknown correlations, and they can only be solved when a turbulence model is formulated that prescribes these correlations.

The present numerical solution of the problem utilizes the CHAMPION 2/E/FIX computer code of Pun and Spalding [11]. This code uses the $k \sim \varepsilon$ turbulence model of Launder and Spalding [12] as well as the SIMPLE algorithm as described by Patankar and Spalding [13].

[11] Pun, W.M., and Spalding, D.B., "A General Computer Program for Two-Dimensional Elliptic Flows," Imperial College Mechanical Engineering Department Report No. HTS/76/2.

[12] Launder, B.E., and Spalding, D.B., "The Numerical Computation of Turbulent Flows," Computer Methods in Applied Mechanics and Engineering, Vol. 3, pp. 269-289, 1974.

[13] Patankar, S.V., and Spalding, D.B., "A Calculation Procedure for Heat, Mass and Momentum Transfer in Three-Dimensional Parabolic Flows," International Journal of Heat and Mass Transfer, Vol. 15, pp. 1787-1806, Pergamon Press, 1972.

The steady-state, time-averaged, two-dimensional governing equations, written here in cylindrical-coordinates, have the following form.

Continuity:

$$\frac{\partial}{\partial x}(\rho u) + \frac{1}{r}\frac{\partial}{\partial r}(\rho v r) = 0 \tag{52}$$

x-Momentum:

$$\frac{\partial}{\partial x}(\rho u^2) + \frac{1}{r}\frac{\partial}{\partial r}(r\rho vu) - \frac{\partial}{\partial x}(\mu \frac{\partial u}{\partial x}) - \frac{1}{r}\frac{\partial}{\partial r}(r\mu \frac{\partial u}{\partial r})$$

$$= -\frac{\partial P}{\partial x} + \frac{\partial}{\partial x}(\mu \frac{\partial u}{\partial x}) + \frac{1}{r}\frac{\partial}{\partial r}(\mu r \frac{\partial v}{\partial x})$$

$$-\frac{2}{3}\frac{\partial}{\partial x}\{\mu[\frac{\partial u}{\partial x} + \frac{1}{r}\frac{\partial}{\partial r}(rv)]\} \tag{53}$$

r-Momentum:

$$\frac{\partial}{\partial x}(\rho uv) + \frac{1}{r}\frac{\partial}{\partial r}(r\rho v^2) - \frac{\partial}{\partial x}(\mu \frac{\partial v}{\partial x}) - \frac{1}{r}\frac{\partial}{\partial r}(\mu r \frac{\partial v}{\partial r})$$

$$= -\frac{\partial P}{\partial r} + \frac{\partial}{\partial x}(\mu \frac{\partial u}{\partial r}) + \frac{1}{r}\frac{\partial}{\partial r}(\mu r \frac{\partial v}{\partial r})$$

$$-\frac{2}{3}\frac{\partial}{\partial r}\{\mu[\frac{\partial u}{\partial x} + \frac{1}{r}\frac{\partial}{\partial r}(rv)]\} - \frac{2\mu v}{r^2} \tag{54}$$

Turbulent energy:

$$\frac{\partial}{\partial x}(\rho uk) + \frac{1}{r}\frac{\partial}{\partial r}(\rho rvk) - \frac{\partial}{\partial x}(\frac{\mu+\mu_t}{\sigma_k}\frac{\partial k}{\partial x}) - \frac{1}{r}\frac{\partial}{\partial r}(r\frac{\mu+\mu_t}{\sigma_k}\frac{\partial k}{\partial r})$$

$$= G_k - \rho\varepsilon \tag{55}$$

Turbulent dissipation:

$$\frac{\partial}{\partial x}(\rho u \varepsilon) + \frac{1}{r}\frac{\partial}{\partial r}(\rho r v \varepsilon) - \frac{\partial}{\partial x}\left(\frac{\mu+\mu_t}{\sigma_\varepsilon}\frac{\partial \varepsilon}{\partial x}\right) - \frac{1}{r}\frac{\partial}{\partial r}\left(r\frac{\mu+\mu_t}{\sigma_\varepsilon}\frac{\partial \varepsilon}{\partial r}\right)$$

$$= C_1 \varepsilon G_k/k - C_2 \rho \varepsilon^2/k \qquad (56)$$

with

$$G_k \equiv \mu_t\{2[(\partial u/\partial x)^2 + (\partial v/\partial r)^2 + (v/r)^2]$$

$$+ (\partial u/\partial r + \partial v/\partial x)^2\} \qquad (57)$$

and

$$\mu_t = C_D \rho k^2/\varepsilon \qquad (58)$$

where μ is the fluid viscosity, μ_t is the turbulent viscosity, k is the kinetic energy of turbulence, and ε is the rate of dissipation of k.

The turbulence model given in Equations (55) and (56) contains five empirical coefficients. Table 1 gives the values of the coefficients used by Pun and Spalding in the 2/E/FIX code.

Table 1. Values of turbulence coefficients.

C_D	C_1	C_2	σ_k	σ_ε
0.90	1.43	1.92	1.00	1.30

The 2/E/FIX code was used to compute the two-dimensional mean velocity field downstream of the step in our flow facility. As an input to the program the velocity profile in the upstream channel at the step location is required. The profile was obtained by fitting a symmetric profile to the pitot tube measurements taken in the central plane of the channel upstream of the step. Both the pitot tube measurements and the assumed profile for the computer program are shown in Figure 33.

Figure 34 shows the computational results in terms of ψ^*, the non-dimensional stream function. Note the difference between the horizontal and vertical scales in Figure 34. The recirculation zone is clearly defined and reattachment occurs at about five step heights downstream of the step. The convergence criterion was 10^{-3} and the solution converged after 468 iterations.

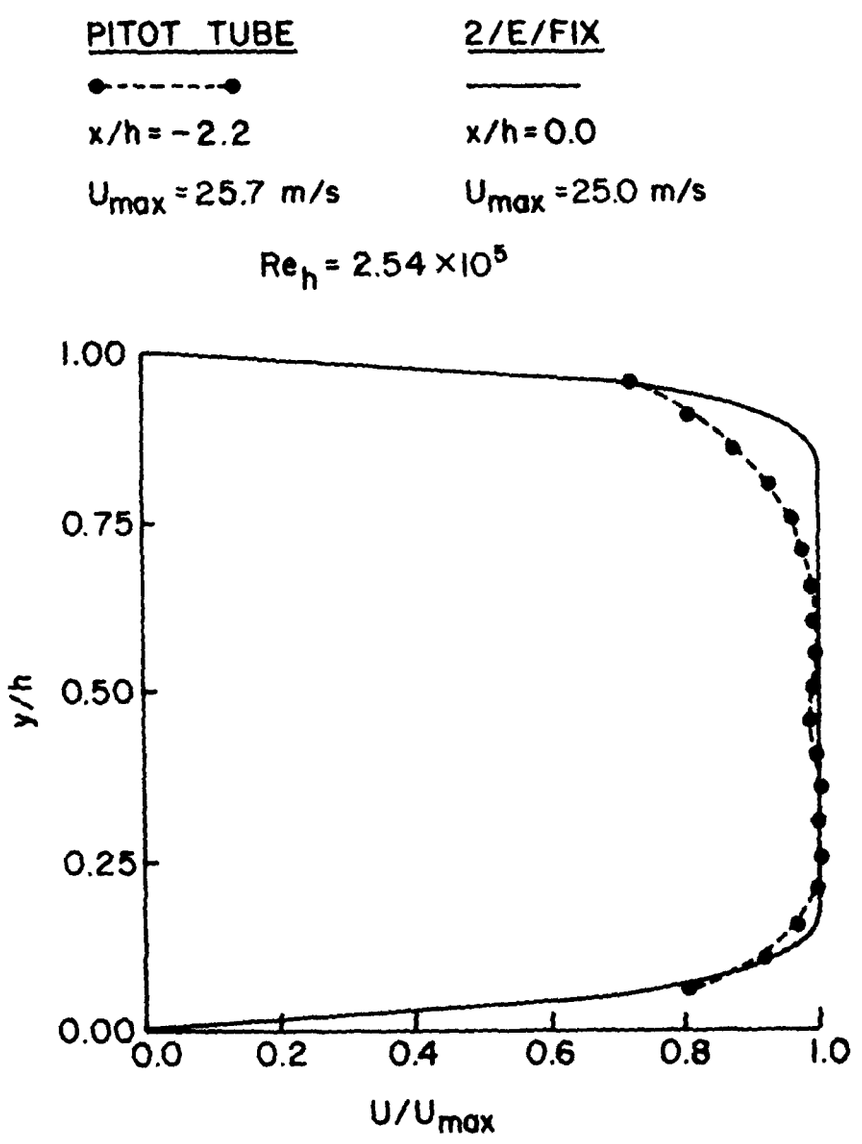

Figure 33. Pitot-tube and 2/E/FIX u/u_{max} Profiles.

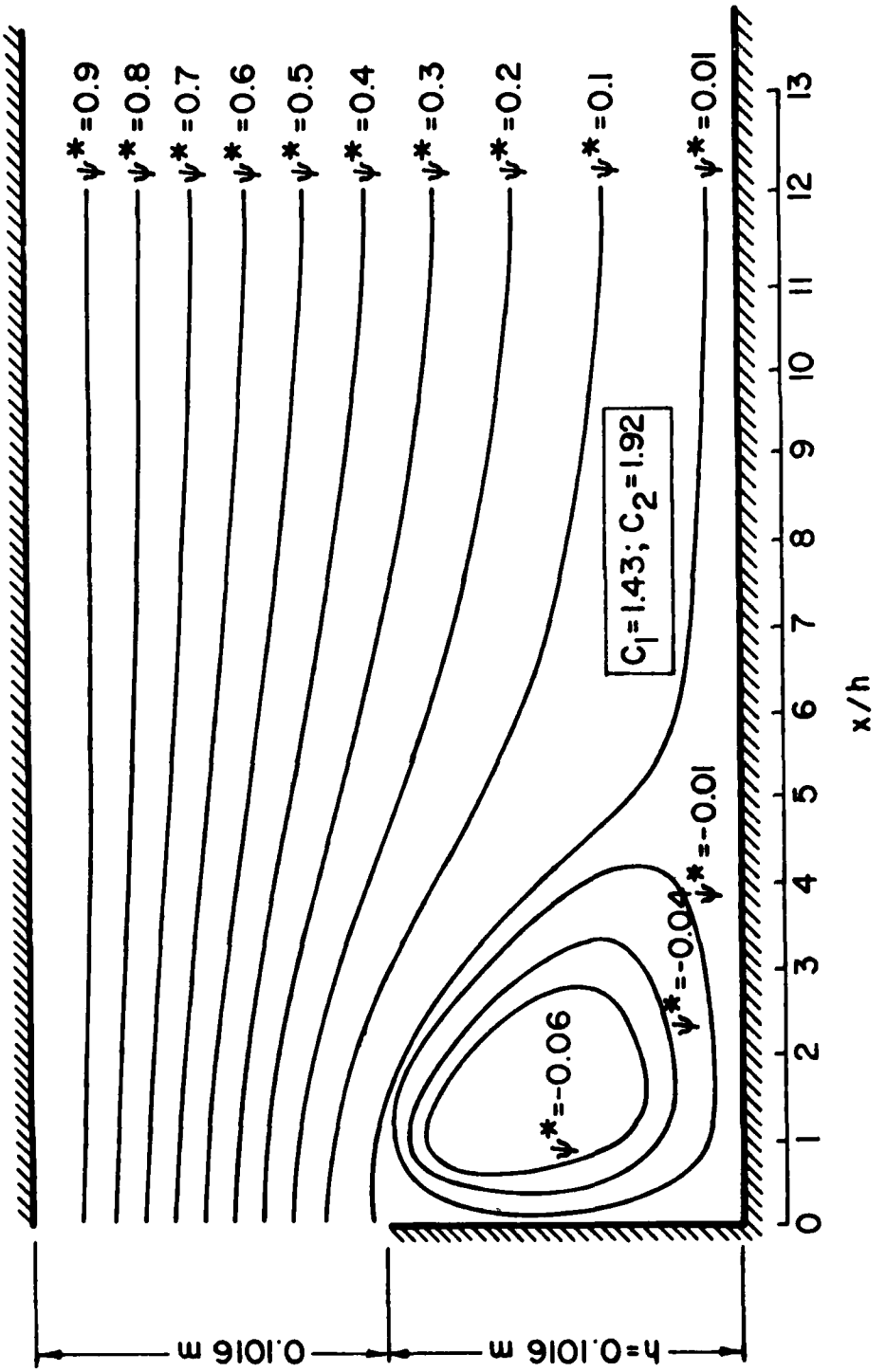

Figure 34. Mean Non-dimensional Streamlines

The flow reattachment point occurs sooner than experimental results found in the literature would indicate. That is, the $k \sim \varepsilon$ turbulence model has inadequately described what is happening to the flow in terms of turbulence production and dissipation. Moon and Rudinger [14] found that a very similar numerical solution failed to match their experimental results also, showing that the turbulence constants listed in Table 1 are not universal. By manipulating the values of C_1 and C_2 they were able to match the predicted reattachment point with their experimental value.

Moon and Rudinger suggested values of 1.44 and 1.70 for C_1 and C_2 respectively. When these values were used in our model the flow field shown in Figure 35 was obtained. The size of the recirculation zone was increased and the reattachment point was moved to about 8.5 step heights downstream. This agrees with the range of 7-9 step heights found in previous measurements [15]. The conclusion is that adjustment of the turbulence coefficients can significantly affect the computed flow field. In the present case only the effect on the reattachment point has been considered. When LDV measurements of the flow are completed it will be possible to determine which choice of coefficients provides the best match for the overall flow field.

2. Experimental Pressure Measurements

Static pressure measurements have been made in the rearward-facing step model as part of the overall flow field measurements. The model consists of a 4" x 4" plexiglass duct expanding to a 4" x 8" duct over a 4" rearward-facing step. Static pressure taps have been placed along the centerline of the bottom of the duct with some placed 1/2" off the centerline.

The pressure readings were made with a 36 bank manometer inclined at 18° with the horizontal. This allowed the resolution of the manometer to be 0.785 mm H_2O per division. Due to the number of tubes and flow unsteadiness, 35 mm slides of the manometer bank were taken to obtain instantaneous pressure measurements. Subsequently, the slides were viewed and the actual readings recorded. Before each slide was taken, the main flow velocity upstream of the step, U_o, was measured with a pitot-tube and adjusted as necessary to ensure a constant flow velocity.

---

[14] Moon, L.F., and Rudinger, G., "Velocity Distribution in an Abruptly Expanding Circular Duct," ASME Journal of Fluids Engineering, Vol. 99, pp. 226-230, March, 1977.

[15] Abbott, D.E., and Kline, S.J., "Experimental Investigation of Subsonic Flow Over Single and Double Backward Facing Steps," Journal of Basic Engineering, Vol. 84, pp. 317-325, September, 1962.

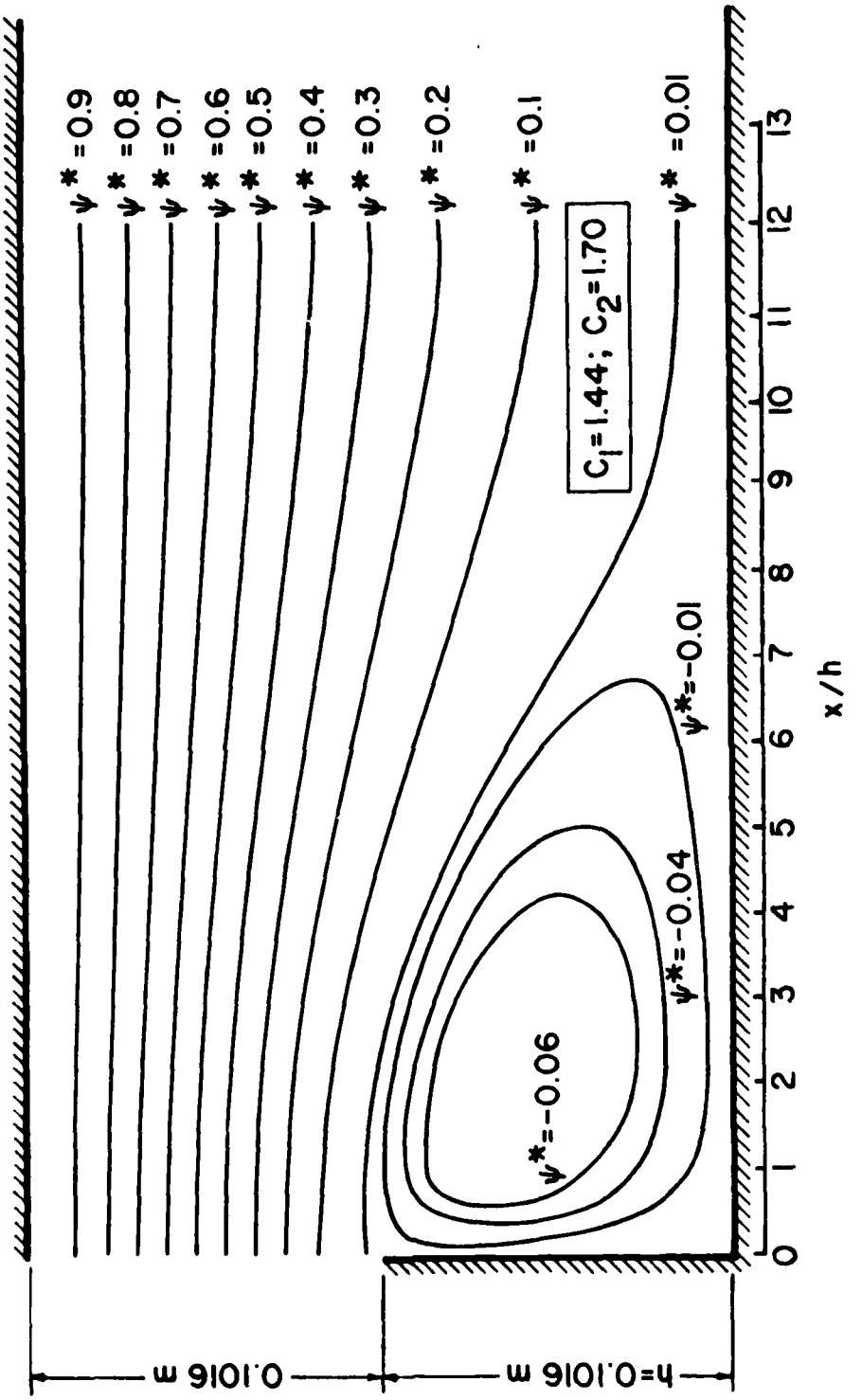

Figure 35. Mean Non-dimensional Streamlines

Figure 36 shows the pressure coefficient distribution for the rearward facing step. In this result, the distance x measured along the surface is non-dimensionalized in terms of the step height h, and the static pressure P is represented in terms of the pressure coefficient, $C_p = (P - P_0)/\frac{1}{2}\rho U_0^2$, where ρ is the air density, and P_0 and U_0 are the static pressure and main-flow velocity respectively at a location 7 inches upstream of the step. Upstream of the step C_p shows a declining tendency with all six runs yielding similar results. Downstream of the step the instability of the flow becomes somewhat pronounced. The pressure observed on the manometer was comparatively steady for each experimental run, but repeated measurements yielded slightly different pressure distributions, indicating the possibility of more than one type of flow pattern under the same inlet conditions. However, the difference in pressure distribution was small. The average C_p values for the six runs taken are also shown in Figure 36.

It can be noted in Figure 36 that for all cases, there is a negative pressure coefficient on the step face (x/h = 0), followed initially by a slight drop downstream of the step, and then a rather rapid rise indicating the approaching reattachment point. The static pressure was measured at three locations on the step face and was constant for all six runs.

Figure 36 agrees fairly well with the data of Tani, Iuchi, and Komoda [16] who did a similar experiment on a rearward-facing step. Their data are shown in Figure 37. They found the pressure coefficient distribution to be rather insensitive to changes in step height. In particular, the pressure coefficient at the base was essentially the same for different step heights except for very low steps, and the rise by reattachement increased slightly as the height increased. The velocity U_0 of Tani et al. was 28 m/s, 3 m/s faster than the results of Figure 36. Also, their model was in a wind tunnel with the wall opposite the bottom of the step at least 55 cm away compared to our model which has the wall 20.32 cm away. This could account for our downstream pressure coefficient not showing a decrease even after 8 step heights downstream.

Tani et al. found their reattachment point to be about 7 step heights downstream of the step or just after the maximum value of C_p had been reached. Based on their results, a possible conclusion about the reattachment point in our model is that it occurs somewhere after 9 step heights downstream, which is in reasonable agreement with computational results discussed in the previous section.

---

[16] Tani, I., Iuchi, M., and Komoda, H., "Experimental Investigation of Flow Separation Associated with a Step or Groove," Aeronautical Research Institute, University of Tokyo, Report No. 364, pp. 119-137, April, 1961.

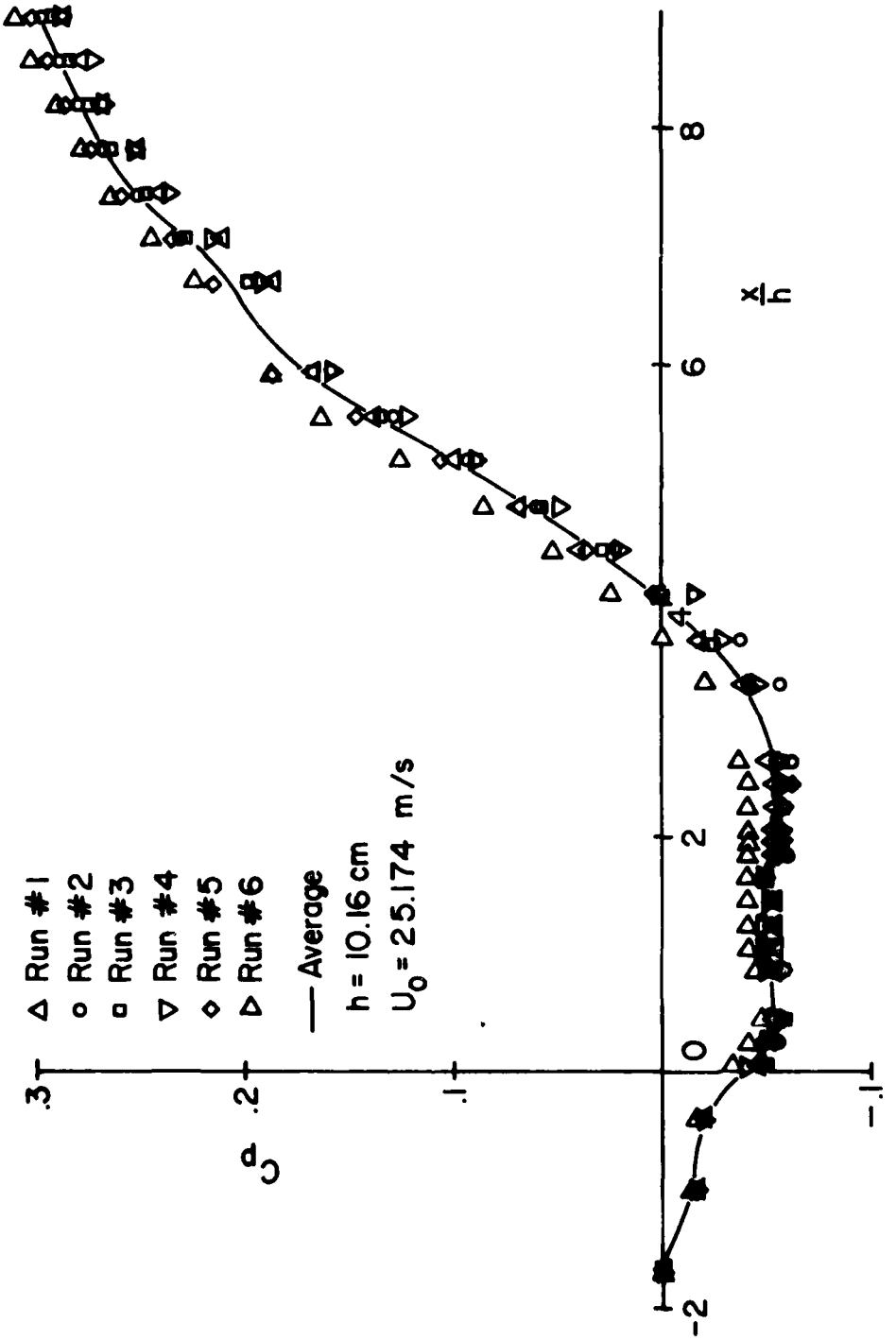

Figure 36. C_p vs x/h for Flow over a Rearward Facing Step

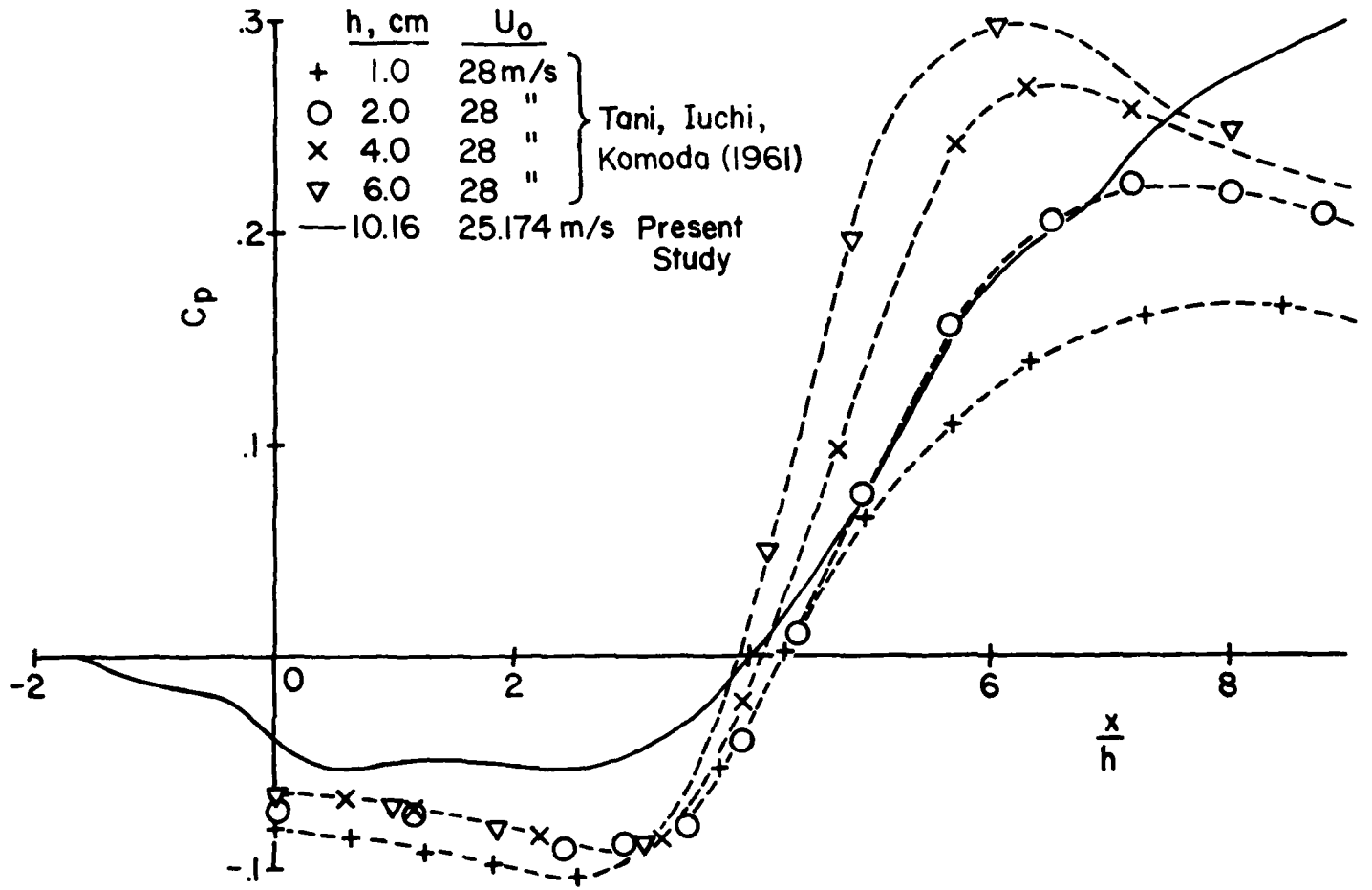

Figure 37. C_p vs x/h for Flow over a Rearward Facing Step

SECTION VI

CONCLUSIONS AND RECOMMENDATIONS

The flexible LDV system designed for the study of biasing errors has performed satisfactorily. Using the alignment procedure described in Section II very precise control of probe volume characteristics is possible. Continuing study of the biasing problem during the coming months will make full use of the system's capabilities.

Preliminary measurements of velocity bias errors using a variable seeding density technique indicate that such a bias does exist, at least in the flow studied, and its magnitude is predicted reasonably well by the correction proposed by McLaughlin and Tiederman. Further measurements under different flow conditions are needed to verify the generality of these results.

A computer model for the flow based on the CHAMPION 2/E/FIX program of Pun and Spalding has been developed. With proper choice of coefficients the flow reattachment point predicted by the model is in reasonable agreement with results of earlier experimental studies by others. Static pressure measurements on the tunnel wall are also in line with data from previous studies. During the next several months LDV measurements will be made throughout the flow field permitting a more definitive comparison between computer model predictions and the actual flow. The investigation will also be extended to an axisymmetric flow simulating a dump combustor.

REFERENCES

[1] Stevenson, W.H. and Thompson, H.D., "Laser Velocimeter Measurements in Turbulent and Mixing Flows," AFAPL-TR-79-2009, March 1979.

[2] Suzaki, Yasuzi and Tachibana, Atsushi, "Measurements of μm Sized Radius of Gaussian Laser Beam Using the Scanning Knife-Edge," Applied Optics, Vol. 14, No. 12, December 1975.

[3] Weicher, H. and Pedrotti, L.S., "A Summary of Useful Laser Equations an LIA Report," Air Force Institute of Technology, Wright Patterson AFB.

[4] Logan, S.E., "A Laser Velocimeter for Reynolds Stress and Other Turbulence Measurements," AIAA Journal, Vol. 10, No. 7, pp. 933-935, 1972.

[5] Logan, S.E., "A Laser Velocimeter Measurement of Reynolds Stress and Turbulence in Dilute Polymer Solutions," Ph.D. Thesis, California Institute of Technology, 1972.

[6] Thompson, H. and Flack, R., Jr., "An Application of Laser Velocimetry to the Interpretation of Turbulent Structure," Proceedings of the ISL/AGARD Workshop on Laser Anemometry, German-French Research Institute, Pfeifer, H. and Haertig, J., Editors, St. Louis, France, p. 189, 1976.

[7] McLaughlin, D. and Tiederman, W., "Biasing Correction for Individual Realization of Laser Anemometer Measurements in Turbulent Flows," The Physics of Fluids, Vol. 16, No. 12, p. 2082, December 1973.

[8] Quigley, M., and Tiederman, W., "Experimental Evaluation of Sampling Bias in Individual Realization Laser Anemometry," AIAA Journal, Vol. 15, No. 2, p. 266, February 1977.

[9] Giel, T. and Barnett, D., "Analytical and Experimental Study of Statistical Bias in Laser Velocimetry," Laser Velocimetry and Particle Sizing, Hemisphere Publishing Corporation, p. 86, 1979.

[10] Bogard, D. and Tiederman, W., "Experimental Evaluation of Sampling Bias in Naturally Seeded Flows," Laser Velocimetry and Particle Sizing, Hemisphere Publishing Corporation, p. 100, 1979.

[11] Pun, W.M., and Spalding, D.B., "A General Computer Program for Two-Dimensional Elliptic Flows," Imperial College Mechanical Engineering Department Report No. HTS/76/2.

[12] Launder, B.E., and Spalding, D.B., "The Numerical Computation of Turbulent Flows," Computer Methods in Applied Mechanics and Engineering, Vol. 3, pp. 269-289, 1974.

[13] Patankar, S.V., and Spalding, D.B., "A Calculation Procedure for Heat, Mass and Momentum Transfer in Three-Dimensional Parabolic Flows," International Journal of Heat and Mass Transfer, Vol. 15, pp. 1787-1806, Pergamon Press, 1972.

[14] Moon, L.F., and Rudinger, G., "Velocity Distribution in an Abruptly Expanding Circular Duct," ASME Journal of Fluids Engineering, Vol. 99, pp. 226-230, March, 1977.

[15] Abbott, D.E., and Kline, S.J., "Experimental Investigation of Subsonic Flow Over Single and Double Backward Facing Steps," Journal of Basic Engineering, Vol. 84, pp. 317-325, September, 1962.

[16] Tani, I., Iuchi, M., and Komoda, H., "Experimental Investigation of Flow Separation Associated with a Step or Groove," Aeronautical Research Institute, University of Tokyo, Report No. 364, pp. 119-137, April, 1961.

[17] Durao, D. and Whitelaw, J.H., "The Influence of Sampling Procedures on Velocity Bias in Turbulent Flows," Proceedings of the LDA Symposium, Copenhagen, p. 138, 1975.

[18] Barnett, D.O. and Bentley, H.T., "Statistical Bias of Individual Realization Laser Velocimeters," Proceedings of the Second International Workship on Laser Velocimetry, Purdue University, March 1974.

[19] Hoesel, W. and Rodi, W., "New Biasing Elimination Method for Laser Doppler Velocimeter Counter Processing, Review of Scientific Instruments, Vol. 48, No. 7, p. 910, 1977.

[20] Johnson, D.A., Bachalo, W.D., and Moddaress, D., "Laser Velocimetry Applied to Transonic and Supersonic Aerodynamics," AGARD Conference Proceedings No. 193 on Applications of Non-Intrusive Instrumentation in Fluid Flow Research, 1976.

[21] Dimotakis, P.E., Collins, D.J., and Lang, D.B., "Laser Doppler Velocity Measurements in Subsonic Transonic, and Supersonic Turbulent Boundary Layers," Laser Velocimetry and Particle Sizing, Hemisphere Publishing Corporation, p. 208, 1979.

[22] Meyers, J.F. and Clemmons, J.I., Jr., "Processing Laser Velocimeter High-Speed Burst Counter Data," Laser Velocimetry and Particle Sizing, Hemisphere Publishing Corp., p. 300, 1979.

APPENDIX

A REVIEW OF VELOCITY BIAS STUDIES

Following the analytical prediction of velocity bias by McLaughlin and Tiederman [7], a number of investigators conducted experiments specifically to verify the existence of this effect. Other investigators made measurements in turbulent flows where the bias should be present and considered it in their data reduction. All of these studies are reviewed here to illustrate the various techniques used and the nature of the results.

Durao and Whitelaw [17] proposed that random sampling of the data record from a burst processor (counter) would remove velocity bias "by diminishing the weighting of signals which appear with small time intervals between them." Computer predictions supported this argument, but measurements on the centerline of a free jet at 25% turbulence intensity were inconclusive. Additional measurements at 40% and 100% turbulence were also not definitive. The concept of random sampling the random (in time) data typical of burst processors as a method of eliminating velocity bias appears questionable in any case.

Quigley and Tiederman [8] made measurements in the viscous sublayer of a water channel. When their velocity profile was corrected using the McLaughlin-Tiederman (M-T) one-dimensional correction (about 10% in this case), their results agreed quite well with the profile predicted from pressure drop measurements. However, when later measurements were made by Bogard and Tiederman [10] in the same channel neither the corrected nor the uncorrected profiles agreed with the predicted profile. Bogard and Tiederman did show that particle arrival rate did not affect the measured mean velocity as had been suggested by Barnett and Bentley [18]. They also showed that possible signal detection probability differences between slow and fast particles due to the lower number of photons scattered by fast particles had no effect on the results. This had been suggested as an effect which might compensate for the velocity bias error.

Hoesel and Rodi [19] proposed a probe volume residence time correction for uniformly seeded flows and a particle separation time correction for nonuniformly seeded flows when the average particle separation time is small compared to the

---

[17] Durao, D. and Whitelaw, J.H., "The Influence of Sampling Procedures on Velocity Bias in Turbulent Flows," Proceedings of the LDA Symposium, Copenhagen, p. 138, 1975.

[18] Barnett, D.O. and Bentley, H.T., "Statistical Bias of Individual Realization Laser Velocimeters," Proceedings of the Second International Workshop on Laser Velocimetry, Purdue University, March 1974.

[19] Hoesel, W. and Rodi, W., "New Biasing Elimination Method for Laser Doppler Velocimeter Counter Processing, Review of Scientific Instruments, Vol. 48, No. 7, p. 910, 1977.

time scale of turbulent fluctuations. This was an attempt to generalize the M-T correction to cases where the instantaneous velocity vector can be at large angles to the mean flow direction as in the highly turbulent region near the edge of a free jet. Hoesel and Rodi made measurements across such a jet. They found that the M-T correction agreed with their correction near the axis, but deviated toward the edges as predicted. However, they had no independent measurement so it is impossible to make any judgement as to whether a bias actually existed. It is interesting to note that the difference between corrected and uncorrected velocities diminished to almost zero as the radial point of measurement increased, so there was really little difference between the two correction schemes over the entire flow.

Giel and Barnett [9] made measurements in a jet flow very similar to that of Hoesel and Rodi. A hot wire was used for comparison. They found no evidence of velocity bias, even though an error on the order of 10% was expected near the axis. There was also no evidence of bias in computed turbulence intensities. They could reach no definite conclusions as to why no bias occurred.

Johnson, Bachalo, and Moddaress [20] reported measurements in a Mach 2.9 separated boundary layer and in the transonic flow past an airfoil; they also found no evidence of velocity bias. A pitot tube was used for comparison in the separated boundary layer study and velocities were computed from static pressure data in the airfoil measurements. They claim that their results support the proposal of Barnett and Bentley that no biasing will occur if the particle arrival rate is much less than the turbulence frequencies. Recall that this conflicts with the experimental results of Bogard and Tiederman.

Dimotakis, Collins, and Lang [21] measured profiles in turbulent boundary layers on a flat plate over a Mach number range from 0.1 to 2.2. A pitot tube was used for comparison. When the LDV measurements were corrected for velocity bias good agreement between the two measurement techniques was obtained.

It is apparent that the velocity bias question is still not resolved. The studies described give conflicting evidence and provide no pattern which would indicate the circumstances under which data should or should not be corrected.

---

[20] Johnson, D.A., Bachalo, W.D., and Moddaress, D., "Laser Velocimetry Applied to Transonic and Supersonic Aerodynamics," AGARD Conference Proceedings No. 193 on Applications of Non-Intrusive Instrumentation in Fluid Flow Research, 1976.

[21] Dimotakis, P.E., Collins, D.J., and Lang, D.B., "Laser Doppler Velocity Measurements in Subsonic Transonic, and Supersonic Turbulent Boundary Layers," Laser Velocimetry and Particle Sizing, Hemisphere Publishing Corporation, p. 208, 1979.

A partial resolution of this dilemma may lie in the "Bragg bias" concept suggested by Meyers and Clemmons [22]. They pointed out that when a Bragg cell is used to upshift the detected signal frequency, the probability of obtaining multiple data samples from the same particle increases. This is due to the fact that the number of cycles required by the processor for validation will occur in a shorter time interval and the processor may reset quickly enough to provide additional data samples before the particle leaves the probe volume. This biases the measured mean velocity to lower values and thus tends to compensate for velocity bias. If the fringe velocity (induced by the Bragg shift) exceeds the particle velocities by a significant amount, it can be shown that the net correction approaches zero and a simple arithmetic mean of the data samples yields the true mean velocity.

Obviously velocity bias compensation due to the Bragg bias effect will exist only if the data processing scheme is such that multiple samples can be obtained from single particles. This depends on particle residence time, Bragg shift, the type of signal processor, and the manner in which computer sampling of the processor output is accomplished. Velocity bias would also be absent if sampling was essentially done at equal time intervals. Unfortunately insufficient information is available in most of the publications cited above to make any meaningful statements about these possible explanations for the observed discrepancies. The technique presented in this report offers the possibility of directly indicating the presence and magnitude of velocity bias errors. When the measurements are complete we hope to be in a position to draw definitive conclusions which will be of general utility to those making LDV measurements in turbulent flows.

---

[22] Meyers, J.F. and Clemmons, J.E., Jr., "Processing Laser Velocimeter High-Speed Burst Counter Data," Laser Velocimetry and Particle Sizing, Hemisphere Publishing Corp., p. 300, 1979.

*U.S.Government Printing Office: 1980 — 657-084/680


ILMED
8